5
21
22
23
27

Numerical Modeling of Oil Containment By a Boom [1]

by Stéphan T. Grilli, Zhimin Hu, and Malcolm L. Spaulding

Department of Ocean Engineering
University of Rhode Island Narragansett, RI 02882, USA

Abstract

This work is part of a research project, funded by the U.S. Coast Guard [2], aimed at developing a hydrodynamic model of *oil containment* by booms. The main goal of the project is to use the model to analyze oil containment failure mechanisms causing substantial loss of oil under the boom. Due to its more catastrophic nature, the failure mode referred to as *critical accumulation* is the main object of the study.

An extensive literature review was conducted for interfacial instabilities between two fluids and for oil containment failure problems. Based on this review, a hierarchy of modeling strategies was proposed. The Phase I model was developed, implemented, and tested as part of this project. Other models are being developed as continuations of this project.

The Phase I model uses piecewise-constant vortex sheets (VS) to represent the oil-water interface in a contained oil slick. Biot-Savart's law is used to calculate flow velocities induced by vorticity distributions in the VSs. An evolution equation is derived for time updating vorticity along VSs, including the effects of inertia, gravity, oil and water density differences, and surface tension at the interface. Higher-order modeling of the VS's geometry is introduced, based on 4th-order sliding polynomials and cubic splines.

The idealized case of a periodic Kelvin-Helmholtz instability is first solved to test and validate the principal numerical algorithms in the model. The pure headwave instability case (i.e., without a boom) is then solved. Model calculations are found to be both stable and accurate. Computational results are qualitatively similar to other published results. Applications of the model to more realistic cases of oil containment by a boom are then presented.

---

[1] In *Proc. 19th Arctic and Marine Oilspill Program Tech. Seminar* (AMOP, Calgary, Alberta, CANADA, June 96), pps. 343-376. Environment Canada, Canada.

[2] *Oil Pollution Research Grant Program*, U.S. Department of Transportation, Grants No. DTRS57-94-G-00076 (FY94) and DTRS57-95-G-00065 (FY95).

1 Introduction and literature review

1.1 Overview

Booms are one of the most commonly used techniques to collect and contain oil on the sea surface, or to protect specific areas against slick spreading by containment or diversion. In the collection mode, floating boom systems are deployed on the free surface, usually in a U or V configurations, and towed towards the oil slick. In the diversion mode, they are used to direct oil to the shoreline or sheltered area.

The containment of oil by a boom is illustrated by the sketches in Fig. 1 which correspond to both an *ocean situation* in which a boom is towed by a boat at speed U over an essentially non-moving water mass (zero current), and a *river situation* in which a fixed boom is placed across a river flow with current U. In both cases, oil accumulates inside the boom with the maximum accumulation occurring at the boom catenary's apex, where the maximum relative water velocity also occurs. Considering the location of accumulation and the small curvature of the boom geometry around the apex point, it is often acceptable (as a first approximation) to simplify this essentially three-dimensional problem to a *two-dimensional* one in the vertical plane intersecting the boom's apex (Fig. 2). It is also reasonable to assume that, for both cases in Fig. 1, the boom does not move and the water flows under the boom at a velocity U, equal to the relative boom-water velocity.

In order to collect as much oil as possible in the shortest possible time, it is desirable to have a tow velocity as large as possible. Various hydrodynamic instabilities at the oil–water interface, however, contribute to a fairly low practical limit for the tow velocity, on the order of 0.5 m/s. In fact, for the idealized problem sketched in Fig. 2, laboratory observations show that interfacial waves start developing at the oil–water interface for relative current speeds, $U \simeq 0.15$ m/s. For larger speed, these waves grow unstable and, in most cases, lead to substantial or even total loss of oil under the boom (Agrawal and Hale [1], Lau and Kirchifer [20], Wicks [27], Wilkinson [28, 29]). In the literature, such instabilities are referred to as *boom containment failure modes* and three main types of containment failures have thus far been identified [3],

- **Drainage Failure** : An increase in relative water-boom velocity U leads to an increase in interfacial friction stresses, causing a shortening and a thickening of the slick. An increase in slick thickness beyond the barrier draft d leads to drainage failure.

  Cross and Hoult [7] studied the steady–state profiles of contained oil slicks and formulated an equation for the maximum slick length l as a function of barrier draft d,

  $$l = \frac{156.25\, g\,(1-s)}{U^2}\, d^2 \qquad (1)$$

  where, $s = \rho_o/\rho_w$ (ρ_o being the oil density and ρ_w the water density) and g is the gravitational acceleration. This equation is applicable only for low current speeds and smooth oil-water interfaces. If slick length is larger than l, containment failure will occur by drainage under the boom.

[3]Note that, in addition to these failure modes which occur in calm weather, the effectiveness of the boom in containing oil can be severely limited by the hydrodynamic behavior of both the boom and the slick under extreme weather conditions that may create high seas. These factors will not be considered in the present study.

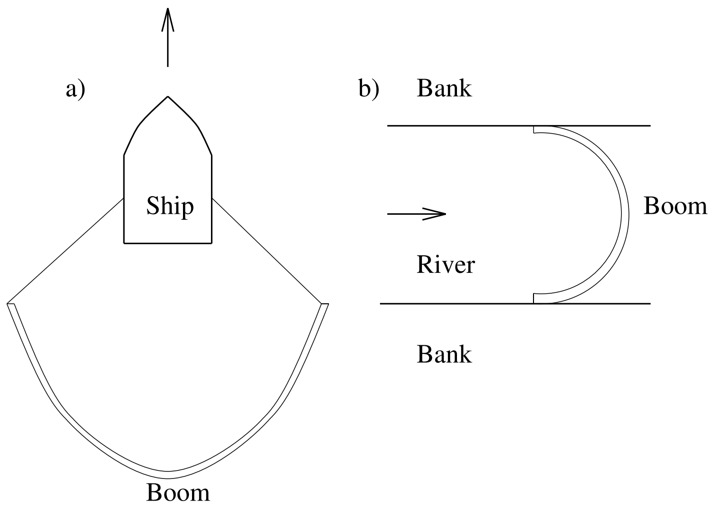

Figure 1: Planview of typical set-up for oil containment by : (a) a towed boom (ocean); or (b) a static boom (river). Arrows mark the direction and magnitude of the relative velocity U between boom and water.

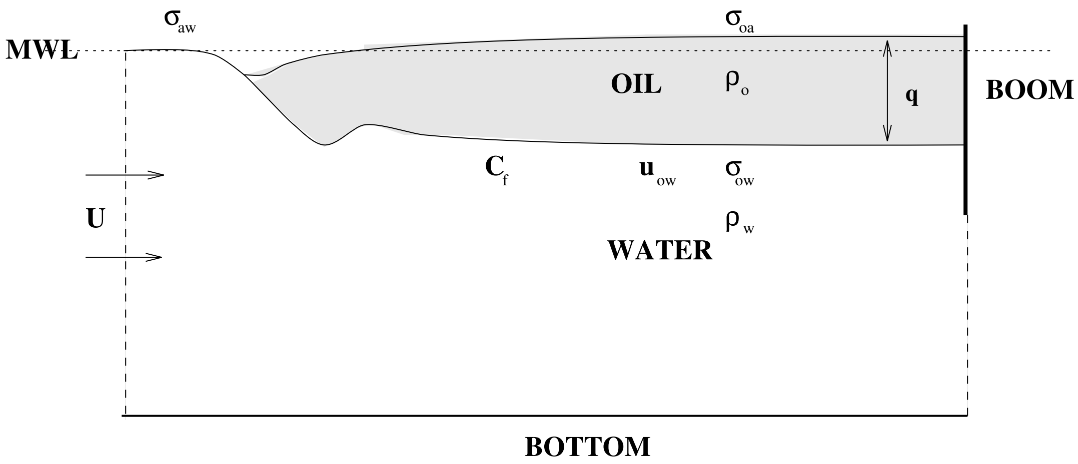

Figure 2: Sketch for initiation of oil containment failure by *critical accumulation*, with mention of important parameters : U, water-boom relative current velocity; $\mathbf{u}_{ow}$, oil-water relative velocity; ρ_o, ρ_w, oil and water density, respectively; σ_{ow}, σ_{oa}, σ_{aw}, interfacial tension coefficients for oil-water, oil-air, and air-water, respectively; C_f, oil-water interfacial friction coefficient; q, oil slick depth; MWL, Mean Water Level.

For larger current speed, the oil-water interface is no longer smooth (see below) and the interfacial friction coefficient C_f increases. For such cases, Delvigne [8] finds empirically that maximum slick length depends on oil volume Q as, $l \propto Q^{2/3}$.

- **Entrainment Failure** : For high relative oil–water velocities and low viscosity oils, $\nu_o < 3,000$ cs, large interfacial stresses occur and induce shear instabilities of the oil-water interface. Such instabilities are characterized by the formation of small fast-moving interfacial waves (ripples) which, for sufficiently large U (on the order of 0.25 m/s), may grow unstable and break, leading to subsequent entrainment of oil droplets in the underlying flow. The droplets either reattach to the slick (if the slick is long enough) or pass under the barrier, leading to *progressive* containment failure by droplet entrainment.

  Significant work on droplet entrainment was done by Agrawal and Hale [1], Leibovich [21] and Wilkinson [28, 29]. Note that drainage and entrainment failure may occur simultaneously in some situations [8].

- **Critical Accumulation** : Prior to Delvigne's [8] experiments, entrainment failure was thought to be the primary dynamic failure mode for contained oil slicks. Delvigne, however, showed that, for oils with large viscosities, $\nu_o \geq 3,000$ cs, another, more catastrophic, failure mechanism always occurs at a lower velocity U than the other two modes. Previous studies did not reveal this failure mechanism because the oil viscosities used in the experiments were too low.

  In this failure mode, referred to as *critical accumulation*, the oil–water interface, when exposed to a relative oil–water flow velocity exceeding a certain critical velocity, $U_{cr} \simeq 0.15$ m/s, develops slow-moving large scale oscillations which eventually cause all of the oil to escape under the barrier, *independent* of barrier draft d.

  A more detailed analysis of Delvigne's experiments reveals that critical accumulation is characterized by the formation of a headwave at the front of the slick (Fig. 3) which grows in amplitude as a function of time and propagates downstream towards the boom. This causes the slick to become both shorter and thicker and eventually leads to almost total loss of oil under the boom. Quite remarkably, for large enough viscosity, Delvigne's experiments show a lack of dependence of U_{cr} on oil viscosity ν_o, density difference, $\Delta\rho_{ow} = \rho_w - \rho_o = \rho_w(1 - s)$, oil volume Q, or water depth h.

  Finally, it should be emphasized that, due to weathering and emulsification, real slicks can quickly reach large viscosities, on the order of 10,000 cs (Johnston *et al.* [17]) and, hence, their containment by a boom is likely to fail by critical accumulation, for tow velocities beyond the critical value.

Many experimental and theoretical studies were pursued in the 1970's to understand the physics of oil containment by a boom and circumstances leading to containment failure. More recently, there has been a renewed interest in studying the problem and attempts made to use numerical modeling tools. An exhaustive literature review was conducted by Grilli *et al.* [14] for the oil containment problem, as part of this project, including qualitative, experimental, and numerical studies. This review clearly showed that interfacial waves occurring during the failure modes discussed above are both initiated and sustained by *shear instability* at the

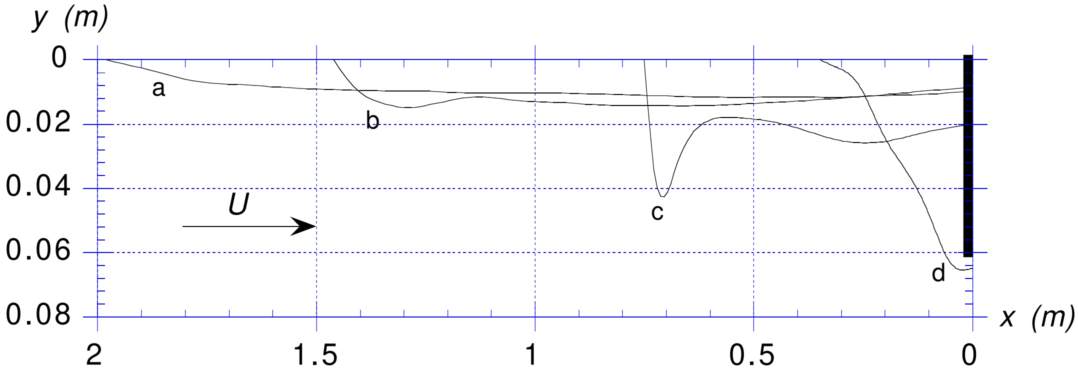

Figure 3: Experimental shapes of oil slicks measured in Delvigne's [8] experiments with Arabian light emulsion ($\nu_o = 2,300$ cs) for relative water-boom velocity U = a : 0.065; b : 0.095; c : 0.128; and d : 0.145 m/s. The figure shows the increase in size of the headwave and the shortening of the slick as U increases from curve a to c and, finally, the failure by critical accumulation with the oil slick draining under the boom in curve d.

oil-water interface, usually referred to as a *Kelvin-Helmholtz (KH) instability* (Benjamin [4], Drazin [10], Jones [18], Rangel and Sirignano [23]).

Hence, modeling KH instability in the context of oil containment by a boom was defined as one of the main objectives of the present study. This is detailed in the next section.

1.2 Statement of the problem

The literature review by Grilli *et al.* [14] identified key parameters and physical phenomena responsible for the three failure modes of oil containment by a boom, discussed above. In the light of Delvigne's [8] and Johnston *et al.*'s [17] experiments, *critical accumulation* seems to be the dominant failure mode for high viscosity oils that are found in many real slicks.

Critical accumulation results from the interplay of the following physical processes and parameters (see Fig. 2),

- the relative *water-boom velocity* U, which controls the magnitude of interfacial friction forces and triggers and sustains KH instability;
- the fluid *density difference* $\Delta\rho_{ow}$, which affects both slick thickness and spreading forces;
- $\Delta\rho_{ow}$ and the *surface tension* at the oil water interface σ_{ow}, which both affect the growth of interfacial KH waves;
- the interfacial *friction coefficient* C_f, which controls the magnitude of interfacial friction forces and thus affects oil slick thickness, and is dependent on interfacial shape (including irregularities due to KH waves);
- *oil viscosity* ν_o, which damps out short interfacial waves and limits the strength of internal circulation cells within the oil slick (hence justifying a quasi-hydrostatic assumption for highly viscous oil slicks).

Other parameters of lesser importance are σ_{aw} and σ_{oa}, the air-water and oil-air surface tension, respectively.

Increasing U or C_f reinforces the KH instability whereas increasing σ_{ow} or $\Delta\rho_{ow}$ (i.e., buoyancy) reduces the instability.

Overall, a steady-sate slick shape can be achieved for $U < U_{cr}$, when stabilizing forces (i.e., spreading forces and circulation in the slick) balance interfacial friction forces. For $U > U_{cr}$, however, increased friction forces at the interface can no longer be compensated by counteracting forces, particularly for high viscosity oils for which circulation in the slick is very limited. Hence, slick length must decrease to balance friction forces and, as a result, interfacial waves grow even larger (see Fig. 3). This, in turn, increases friction forces even more, leading to the unstable reduction in slick length and total loss of oil by drainage under the boom that characterize *critical accumulation*. Delvigne points out that, at the onset of critical accumulation, strong deformations of interfacial waves, headwave, or both are observed (see, e.g., Fig. 3 curve c). [This is confirmed by Johnston *et al.*]. He also notes that, for lower viscosity oils, a similar unstable growth of interfacial waves would probably lead to oil being torn off the wave crests and, therefore, to droplet entrainment.

Hence, modeling KH instability and resulting interfacial waves in the context of oil containment by a boom seems to be the key to both understanding and predicting *critical accumulation* failure. To do so, due to the high degree of complexity of physical mechanisms involved, an "incremental approach" was used in which the initial model developed in this project would only be a first step towards a more comprehensive model of oil containment that could eventually provide practical, useful results. The first model in this incremental approach, referred to as the *Phase I model*, is detailed in the following.

Modeling the problem sketched in Fig. 2 involves solving for the unsteady motion of a two fluid system in the presence of fixed *obstacles* (bottom, boom). This system has both free surfaces (air-oil, air-water) and an *interface* (oil-water), for which viscous and turbulent effects may be important. Apart from the region very close to the oil-water interface, due to the large Reynolds number of the flow, water behaves as an almost perfect *inviscid fluid* (Batchelor [3]). From the literature review, it is apparent that *dynamic effects* dominate along the oil–water interface as far as development of KH instabilities and interfacial waves (Wilkinson [28]). Besides dynamic effects, both slick thickness q and shape also depend, but to a lesser extent, on *viscous/turbulent effects* at both the oil-water interface and within the oil slick (slow viscous circulation occurs within the oil slick; Milgram and Van Houten [22]). *Surface tension* at the interface also plays an important role in the development of KH waves (Di Pietro and Cox [9], Rangel and Sirignano [23]).

Only a very limited number of modeling approaches have been proposed in the literature to represent the motion of contained oil slicks, i.e., the oil–water interface and the underlying water flow. Among the few, it seems that only the work by Zalosh [30] included the important parameters, identified above, that affect interfacial instability phenomena responsible for the *critical accumulation* failure of oil slicks. Zalosh's model, in particular, was the only one where unsteadiness of KH shear instability and the detailed shape of interface was taken into account. This work was based on using inviscid Vortex Sheets (VS) to represent interfacial geometry and vorticity as a function of time. Several unrealistic simplifications and incorrect coefficients in the model equations, however, prevented this model from providing quantitatively realistic results for a sufficiently long time.

Two other models, by Bai and Kim [2] and Clavelle and Rowe [6], concentrated on representing fluid behavior in the bulk of the oil and water domains in front of the boom, and ignored surface tension and KH waves on the oil–water interface. Because domain-discretization-type methods were used in these models (i.e., Finite Difference Method, Finite Volume Method), they also lacked sufficient resolution for the discretization of the oil-water interface geometry. This, however, is the region of the flow where accuracy is most needed in order to correctly model and predict oil containment failure by critical accumulation. Along the same line, Ertekin and Sundararaghavan [12] recently computed viscous flows past a boom. In this study, however, both the oil-thickness and the KH waves at the oil–water interface were totally neglected and the model concentrated on determining the flow below the slick and downstream of the boom. Hence, despite the authors' statement, such a model is unable to predict instabilities at the oil-water interface observed in experiments. Finally, in the last three models, due to the large Reynolds number of the flow below the slick, and in spite of using Navier-Stokes equations, the models actually solve Euler equations and, hence, implicitly assume an *inviscid fluid*.

For an inviscid fluid in which (shear-induced) vorticity is concentrated along interfaces and solid boundaries, vorticity is well represented by vortex sheets (VS) (Batchelor [3]). The analysis of the VS dynamics shows that induced velocities can be expressed by Biot-Savart's law (Lamb [19], Batchelor [3]), which employs a boundary integral formulation. This allows for the development of Boundary Integral Equation (BIE) models which, when combined with higher-order Boundary Element Methods (BEM) for the spatial discretization, have proven to be very efficient and accurate for solving unstable free surface flow and gravity wave problems (e.g., Grilli and Subramanya [15, 16]). More specifically, in BIE/BEM models, discretization of the solution is limited to the boundaries (i.e., to interfaces in the present case) whereas the representation of the solution inside the fluid domain is *exact*. Hence, model grids are very much reduced in size compared to domain-discretization-type methods and high resolution can thus be achieved along the boundaries (and interfaces). Furthermore, for moving boundary problems like the present one, time updating of both the discretization and the boundary conditions is much more efficiently and accurately implemented in BEM models than in domain-discretization-type models where the whole spatial grid has to be recreated at each time step.

In the *Phase I model*, we adopted an *inviscid VS* approach to represent interfaces between the two fluids. Viscous circulation is neglected in the oil slick, i.e., a *quasi-hydrostatic* pressure is assumed, which is acceptable in view of experimental evidence, particularly for high viscosity oils (e.g., Milgram and Van Houten [22]). The VS approach exactly accounts for the vorticity generated by the velocity discontinuity at the oil-water interface but not for the viscous or turbulent diffusion of vorticity that may occur at the interface [4]. The underlying water is assumed to behave as an incompressible *inviscid fluid* (i.e., an ideal fluid).

Equations for the Phase I model are given in Section 2 and applications in Section 3. Possibilities for further development and improvements of this model are discussed in Section 4.

[4]Note that the vorticity along the VSs will induce a slow non-viscous rotational motion in the oil slick, but with likely minimal vertical accelerations. Hence, this is consistent with the assumption that pressure in the oil is close to hydrostatic. Accounting for a slow circulation in the slick would only provide small additional stabilizing forces, which would reduce interfacial waves. The present model is thus likely to slightly overpredict the growth of interfacial instabilities.

2 The mathematical and numerical model

In the Phase I model, VSs are used to represent interfaces (air-water, air-oil, oil-water) and solid boundaries (boom, bottom). Here, the VSs are discretized by *piecewise-constant elements* of vorticity. This, however, already represents an improvement over most existing VS models which use less accurate point vortices (e.g., Zalosh [30, 31], Rangel and Sirignano [23]). The *velocity induced* by the VSs will be calculated based on Biot-Savart's law (Batchelor [3]).

Time evolution of the VSs will be computed using an equation that accounts for the oil-water density difference, interfacial tension effects, and gravity effects (Fink and Soh [13], Rangel and Sirignano [23], Zalosh [30, 31], Zalosh and Jensen [32], Zaroodny and Greenberg [33]).

Details of model equations and numerical algorithms are given in the following.

2.1 Velocities induced by VSs

For an inviscid fluid flow, when vorticity is concentrated within two-dimensional *vortex sheets* (VS) in a vertical plane (x, y), Biot-Savart's law can be used to calculate the induced velocity (u, v) as (Batchelor [3], p527),

$$\begin{aligned} u(x,y) &= \frac{1}{2\pi}\int \frac{y-y'}{r^2}\,\gamma(s)\,ds \\ v(x,y) &= -\frac{1}{2\pi}\int \frac{x-x'}{r^2}\,\gamma(s)\,ds \end{aligned} \tag{2}$$

where $\gamma(s)$ is the *clockwise* vortex sheet strength (i.e., minus the vorticity) and $s(x', y')$ is the curvilinear abscissa along the sheet.

When points $\boldsymbol{x} = (x, y)$ do not belong to the sheet, integrals in (2) are non-singular. For points (x, y) within the sheet, integrals in (2) are singular for vanishing r and must thus be calculated in a Cauchy Principal Value (CPV) sense. In this case, (2) also takes the form of a Boundary Integral Equation (BIE) for $\boldsymbol{u}(x, y)$ on the sheet.

In the numerical model, discretized expressions of (2) are used to calculate the sheet position as a function of time, according to the Lagrangian definition of velocities,

$$\frac{d\boldsymbol{x}}{dt}(t) = \boldsymbol{u}(x,y) \tag{3}$$

where the time derivative follows the motion of the sheet.

A standard simplifying assumption in studies involving VS dynamics is to assume that the vorticity is either *piecewise constant* or is concentrated at *point vortices* along the sheets. Despite their similarity—and sometimes their confusion in the literature—, these two representations differ in the sense that point vortices do not have a self-induced velocity contribution to Eqs. (2) whereas piecewise constant distributions of vortices do have self-induced velocity at the center of each interval, due to CPV integral contributions in (2) (Fink and Soh [13], Van de Vooren [25]). In many studies, point vortices are found to only give a poor representation of continuous vortex sheets which often quickly leads to inaccurate or even to unstable results, when used to calculate the dynamics of VSs as a function of time. This is true unless point vortices are continuously regridded to equal arc-length distance on the sheet (Fink and Soh [13]). The reason for this will be clear from the following.

Vortex sheets in fact represent a continuous (line) vorticity variation which can be well approximated by a piecewise polynomial distribution of vorticity similar to Boundary Elements used in continuum mechanics (e.g., Brebbia [5]). The simplest possible representation of this type is made of N piecewise-constant elements of vorticity density, $\gamma(s_i) = \gamma_i$.

Doing so, (2) transforms into,

$$\begin{aligned} u_i &= \frac{1}{2\pi}\sum_{j=1}^{N}\gamma_j \int_{s_j-\Delta s_j/2}^{s_j+\Delta s_j/2} \frac{y_i - y}{r_i^2}\, ds \\ v_i &= -\frac{1}{2\pi}\sum_{j=1}^{N}\gamma_j \int_{s_j-\Delta s_j/2}^{s_j+\Delta s_j/2} \frac{x_i - x}{r_i^2}\, ds \end{aligned} \tag{4}$$

for $(i = 1, ..., N)$, with,

$$r_i = \{(x - x_i)^2 + (y - y_i)^2\}^{1/2} \tag{5}$$

Assuming that the geometry within each vortex element is smoothly varying and can thus be approximated by values at mid-point s_i of each element, and denoting by $\Gamma_i = \gamma_i \Delta s_i$ the vorticity attributed to each element i, (4) transforms into a simple summation for $j \neq i$. For $j = i$, however, integrals in (4) are singular and CPV's must be calculated. This can be done using either polar coordinates or complex notations (e.g., Fink and Soh [13]) and we find for $(i = 1, ..., N)$,

$$\begin{aligned} u_i &= \frac{1}{2\pi}\sum_{j\neq i}\frac{y_i - y_j}{r_{ij}^2}\,\Gamma_j + \tilde{u}_i \\ v_i &= -\frac{1}{2\pi}\sum_{j\neq i}\frac{x_i - x_j}{r_{ij}^2}\,\Gamma_j + \tilde{v}_i \end{aligned} \tag{6}$$

where $(\tilde{u}_i, \tilde{v}_i)$ represent CPV's contributions to the velocity (u_i, v_i) given by,

$$\begin{aligned} \tilde{u}_i &= -\frac{1}{2\pi}\frac{\Gamma_i}{\Delta s_i}\,\sin\theta_i\,\log\frac{r_{i+1/2}}{r_{i-1/2}} \\ \tilde{v}_i &= +\frac{1}{2\pi}\frac{\Gamma_i}{\Delta s_i}\,\cos\theta_i\,\log\frac{r_{i+1/2}}{r_{i-1/2}} \end{aligned} \tag{7}$$

where θ_i is the angle between the x-axis and segment i, and $[r_{i-1/2}, r_{i+1/2}]$ denote distances from both extremities to the mid-point of segment i.

It is easy to see in Eq. (7) that the CPV contributions disappear when vortex elements are regridded to equal arclength distance so that $r_{i-1/2} = r_{i+1/2}$. [This was the method used by Rangel and Sirignano [23] to avoid calculating CPV integrals.]. Thus, when regridding is used or when vortex elements do not change too rapidly in length as a function of time, Eq. (4) reduces to the summations in the first terms of its right hand side, which is identical to assuming discrete vortices. When, either regridding is not used or when the length of vortex elements significantly changes with time, CPV's terms (7) provide significant contributions in (6) and the assumption of discrete vortices is unacceptable [5]. This is the likely reason why Zalosh [30, 31],

[5] One would see, for instance, that if elements (i.e., boundary segments) are very much stretched or become very small, CPV terms in (7) provide almost singular (i.e., very large) contributions to (6), whereas discrete vortices approaching each other would not exhibit this behavior.

who used discrete vortices and no regridding, was unable to pursue his computations for a long time without experiencing numerical instability whereas Rangel and Sirignano [23], who also used discrete vortices but performed regridding at each time step, were able to calculate the development of Kelvin-Helmholtz instability and rolling-up of vortex sheets at an interface, for a fairly long time (see Fink and Soh [13] and Van de Vooren [25] for discussions of these and other related problems).

2.2 Rate of change of circulation on the VSs

For a vortex sheet representing the interface between two fluids moving with velocity $\boldsymbol{u}_o$ and $\boldsymbol{u}_1$, respectively, the vortex sheet strength (i.e., vorticity density) is given by [30, 31, 25, 23],

$$\gamma(s) = \Delta u_s = u_{os} - u_{1s} \tag{8}$$

in which,

$$u_{os} = \boldsymbol{u}_o \cdot \boldsymbol{s} \quad ; \quad u_{1s} = \boldsymbol{u}_1 \cdot \boldsymbol{s} \quad ; \quad \boldsymbol{s} = [\cos\beta, \sin\beta] \tag{9}$$

where $\boldsymbol{s}$ is the tangential vector along the sheet and $\beta(s)$ is the angle between the tangent to the sheet and the x-axis [6].

Using (8), the circulation (i.e., vorticity) associated with a small vortex element i of length Δs_i, over which we assume constant velocity and smoothly varying geometry, is given by,

$$\Gamma(s_i) \equiv \Gamma_i = \int_{s_i-\Delta s_i/2}^{s_i+\Delta s_i/2} \gamma(s)\, ds \simeq (\, u_{os} - u_{1s}\,)_i\, \Delta s_i = \gamma_i \Delta s_i \tag{10}$$

For a uniform, incompressible, inviscid fluid with conservative forces, Kelvin's theorem states that the rate of change of circulation around a closed material contour moving with the fluid is zero (e.g., Batchelor [3]),

$$\frac{D\,\Gamma}{D\,t} = 0 \qquad \text{with} \qquad \frac{D}{D\,t} \equiv \frac{\partial}{\partial t} + \boldsymbol{u} \cdot \boldsymbol{\nabla} \tag{11}$$

where D/Dt denotes the material derivative.

For a vortex sheet at the interface between two regions of different velocity within the same fluid, however, Van de Vooren [25] clearly showed that Kelvin's theorem, as stated in (11), is not applicable. Kelvin's theorem may only be applied for a contour moving with the reference velocity, $\boldsymbol{u} = \frac{1}{2}(\boldsymbol{u}_o + \boldsymbol{u}_1)$, equal to the mean between velocities on both sides of the sheet. This reference velocity is defined as the *sheet velocity* and will be used whenever calculating material time derivatives with respect to the sheet motion, referred to as d/dt.

For the interface between two different fluids with density ρ_o and ρ_1, and non-zero interfacial tension σ_{o1}, the fluid is non-uniform and forces are non-conservatives. Hence the rate of change of circulation around a material contour crossing the interface is non-zero and an evolution equation must be developed to predict its behavior. Zaroodny and Greenberg [33] first derived an equation for the rate of change of circulation for a continuous vortex sheet without surface tension. Zalosh [30, 31] developed a similar equation, including surface tension effects, for a

[6] Note that β and θ, introduced earlier, have different definitions but that, for calculations of self-induced velocity of piecewise constant vortex sheet elements, these angles have the same value.

sheet discretized with point vortices but made an error when he failed to consider the difference mentioned above between time derivatives D/Dt, following fluid particles on either side of the sheet, and those d/dt, following the sheet motion. This was later pointed out by Rangel and Sirignano [23] who derived the correct evolution equation, but without including gravitational effects.

The following is a derivation of the rate of change of circulation, including both gravity and surface tension effects at the interface between two fluids, for a vortex sheet with piecewise constant vorticity elements. Taking the material time derivative, of Eq. (10), with (8), we get for the rate of change of circulation associated with a small vortex element of length Δs_i as,

$$\frac{D\,\Gamma}{D\,t}(s_i) \equiv \frac{D\,\Gamma_i}{D\,t} = \int_{s_i-\Delta s_i/2}^{s_i+\Delta s_i/2} \left(\frac{D\,u_{os}}{D\,t} - \frac{D\,u_{1s}}{D\,t}\right) ds \simeq \left(\frac{D\,u_{os}}{D\,t} - \frac{D\,u_{1s}}{D\,t}\right)_i \Delta s_i \tag{12}$$

Tangential accelerations in (12) can be expressed for both fluids using Euler's equations in the $\boldsymbol{s}$ direction as,

$$\frac{D\,u_{os,1s}}{D\,t} = -\frac{1}{\rho_{o,1}}\frac{\partial p_{o,1}}{\partial s} - g\sin\beta \tag{13}$$

in which p denotes the pressure (discontinuous across the interface due to surface tension).

From the definition of the *sheet velocity* $\boldsymbol{u}$ the tangential acceleration following the vortex sheet is obtained as,

$$\frac{du_{si}}{dt} = \frac{1}{2}\left(\frac{du_{os}}{dt} + \frac{du_{1s}}{dt}\right)_i \tag{14}$$

with, according to the definitions of different material derivatives,

$$\frac{d}{dt} = \frac{D}{D\,t} \pm \frac{1}{2}(\boldsymbol{u}_o - \boldsymbol{u}_1)\cdot\boldsymbol{\nabla} \tag{15}$$

with the plus sign being taken in fluid 1 and the minus sign in fluid 0. Introducing Eq. (15) in Eq. (14), we get,

$$\frac{du_{si}}{dt} = \frac{1}{2}\left(\frac{D\,u_{os}}{D\,t} + \frac{D\,u_{1s}}{D\,t}\right)_i - \frac{1}{4}(u_{os} - u_{1s})_i\left(\frac{\partial u_{os}}{\partial s} - \frac{\partial u_{1s}}{\partial s}\right)_i \tag{16}$$

Finally, using Eqs. (8) and (13) for the tangential velocities and Eq. (8) for the vortex sheet strength, we get,

$$\frac{du_{si}}{dt} = -\frac{1}{2}\left(\frac{1}{\rho_o}\frac{\partial p_o}{\partial s} + \frac{1}{\rho_1}\frac{\partial p_1}{\partial s} + 2g\,\sin\beta\right)_i - \frac{1}{4}\gamma_i\frac{\partial\gamma_i}{\partial s} \tag{17}$$

Due to a confusion between different material derivatives, the last term in equation (17) was missing in Zalosh's [30, 31] equations.

From the expression of surface tension effects at the interface between two fluids (Batchelor [3]), the pressure jump across the VS is given by,

$$p_o - p_1 = \sigma_{o1}\frac{1}{\mathcal{R}} \tag{18}$$

in which $1/\mathcal{R}(s)$ is the VS curvature. Using curvilinear coordinates, it can easily be shown that the curvature is identical to, $\partial\beta/\partial s$. Hence, taking the tangential derivative of (18) and, eliminating the material tangential accelerations and the pressure between equations (12), (13), and (17), we finally get the rate of change of circulation at point s_i of the sheet as,

$$\frac{D\,\Gamma_i}{D\,t} = 2\kappa\,\Delta s_i\left(\frac{du_{si}}{dt} + g\,\sin\beta_i + \frac{1}{4}\gamma_i\frac{\partial\gamma_i}{\partial s}\right) - \frac{2\sigma_{o1}}{\rho_o+\rho_1}\,\Delta s_i\,\frac{\partial^2\beta_i}{\partial s^2} \qquad (19)$$

where $\kappa = (\rho_1 - \rho_o)/(\rho_1 + \rho_o)$ is the Atwood number and, by (9),

$$\frac{du_{si}}{dt} = \frac{du_i}{dt}\cos\beta_i + \frac{dv_i}{dt}\sin\beta_i \qquad (20)$$

Equation (19) contains the tangential acceleration along the VS, du_{si}/dt, which is proportional to fluid acceleration components on the sheet (20). In most earlier numerical models of unsteady motion of VSs, accelerations were calculated by backward finite differentiation [30, 31, 32, 23]. As suggested (without detail) by Rangel and Sirignano [24], however, accelerations can also be calculated by direct time differentiation of Biot-Savart's law (2). When carried out under the integral signs following Leibnitz rule, such a differentiation creates terms proportional to both Γ_i and $D\Gamma_i/Dt$. Hence, rates of change of circulation $D\Gamma_i/Dt$ can be iteratively calculated using (19) and this expression of accelerations.

In their time differentiation of (2), however, it is not clear whether Rangel and Sirignano [24] accounted for CPV integrals. In fact, since they avoided calculating such terms for the velocities in Eq. (6) altogether, by using a regridding method, it is likely that they simply calculated accelerations by time differentiating the equivalent [7] of Eq. (2).

Grilli *et al.* [14] calculated accelerations by time differentiation of Eq. (2), assuming a vortex sheet with a piecewise-constant distribution of N vortex elements and taking into account CPV integrals resulting from self-induced velocities. Detailed expressions for these accelerations can be found in [14]. In the numerical model, accelerations will thus be explicitly replaced in (19), as a function of Γ_i and $D\Gamma_i/Dt$, and rates of change of circulation $D\Gamma_i/Dt$ will be explicitly calculated.

2.3 Semi-infinite vortex sheets

As in Zalosh [30], horizontal semi-infinite vortex sheets will be used in the numerical model to represent regions of the water domain with constant uniform horizontal velocity U. In Fig. 4, for instance, this corresponds to free surface and bottom regions both in front of the slick (e.g., from $x = -\infty$ to $x = x_\ell$) and behind the boom (e.g., from $x = x_r$ to $x = +\infty$).

Assuming no air velocity and no flow through the bottom, these semi-infinite sheets have a tangential velocity jump $\Delta u_s = \pm U$, with the negative sign being taken on the free surface and the positive sign on the bottom.

When part of the fluid domain is discretized with piecewise-constant vortex elements, such semi-infinite vortex sheets provide contributions to the discretized form (6) of Biot-Savart's law (2) for the sheet velocity, and also to the VS's accelerations. These contributions were calculated by Grilli *et al.* [14]. For instance, if the unperturbed free surface is at $y = 0$ and the horizontal

[7] Note that in Zalosh [31], Van de Vooren [25], and Rangel and Sirignano [23, 24], periodic problems were solved for which Eq. (2) was replaced by a different expression assuming a spatial periodicity λ, for the interface shape. See Section 3.1.

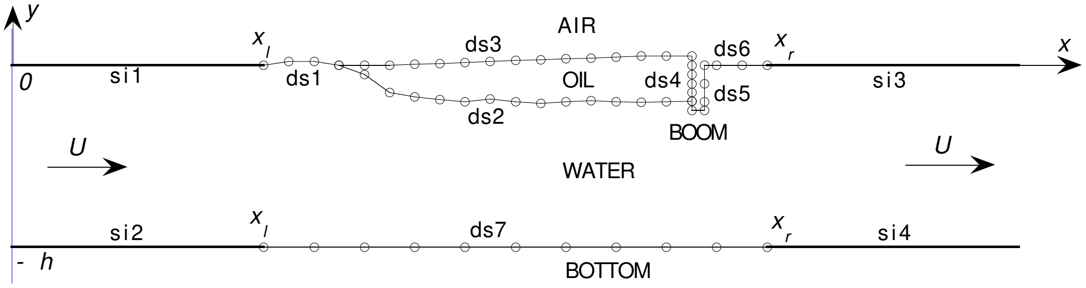

Figure 4: Sketch of computational domain for the oil containment by a boom, with definition of main parameters : U = flow velocity; si1-si4 = semi-infinite vortex sheets; ds1-ds7 = piecewise-constant discretized vortex sheets; $\circ$ = centers of discretized vortex elements.

bottom is at $y = -h$, the total contribution to the velocity of four semi-infinite vortex sheets located at $(x_\ell, 0)$ and $(x_r, 0)$, with strength $-U$, and at $(x_\ell, -h)$ and $(x_r, -h)$, with strength $+U$ can be calculated as,

$$
\begin{aligned}
u_{\ell r} &= \frac{U}{2\pi}\{2\pi + \arctan\left(\frac{x - x_\ell}{y}\right) - \arctan\left(\frac{x - x_\ell}{y+h}\right) - \arctan\left(\frac{x - x_r}{y}\right) \\
&\quad + \arctan\left(\frac{x - x_r}{y+h}\right)\} \\
v_{\ell r} &= \frac{U}{4\pi} \log \frac{[(x - x_r)^2 + y^2]\,[(x - x_\ell)^2 + (y+h)^2]}{[(x - x_\ell)^2 + y^2]\,[(x - x_r)^2 + (y+h)^2]}
\end{aligned}
\tag{21}
$$

As a verification, if we take $x_\ell = x_r$ in Eq. (21), thus assuming a uniform flow represented by two infinite vortex sheets, we can see that (21) indeed reduces to, $u_{\ell r} = U$ and $v_{\ell r} = 0$.

For the accelerations it could be shown, similarly, that all contributions from the four sheets, as expected for a uniform flow, cancel each other and we get, $du_{\ell r}/dt = dv_{\ell r}/dt = 0$.

2.4 The numerical model

Figure 4 gives a sketch of a computational domain that could be used to model oil containment by a boom in finite depth, with definition of various parameters. The geometry of the boundaries and interfaces is represented using both discretized vortex sheets (ds), with piecewise-constant vorticity distribution and continuous semi-infinite horizontal vortex sheets (si), representing regions of the water domain with constant uniform horizontal velocity U (see Section 2.3). Vortex sheet dynamics equations for both of these cases have been detailed before.

Contributions of semi-infinite sheets to flow velocities and accelerations are exactly accounted for in the model, whereas contributions of discretized sheets are numerically calculated as a function of geometry $[(x_i, y_i), \Delta s_i, \theta_i, \beta_i, \partial^2\beta_i/\partial s^2]$ and field variables $[\Gamma_i, d\Gamma_i/dt, (u_i, v_i), (du_i/dt, dv_i/dt)]$ at mid-points of each constant vortex sheet element (boundary element).

Adaptive time stepping method

Assuming that both discretized geometry and field variables are known at time t, the numerical model is used to compute these quantities at time $(t + \Delta t)$ (with Δt being a small time step). This can be done by simultaneously integrating vortex sheet dynamics equations in discretized form, (6), (7), (10), (19), and (20), together with the expressions of induced accelerations and contributions of semi-infinite sheets of the form (21). Computation of an initial steady state solution for the general oil containment problem will not be discussed here but two specific applications are discussed in Section 3.

In earlier models proposed in the literature (Zalosh, [30, 31], Rangel and Sirignano [23, 24]), implicit iterative methods were used for the integration of equations of the form (2), (6) (or equivalent for periodic problems; see Section 3.1) and (19) (or equivalent), together with iterative or backward finite difference approximations of accelerations. These models, however, often exhibited sawtooth instability of the solution which required smoothing of the geometry after each time step (e.g., Zalosh [30]). Such instabilities, we believe, are partly due to the lack of representation of self-induced velocities of vortex elements (see discussion above) and to the implicit iterative scheme used in the models. In the present study, CPV integrals are exactly accounted for and, hence, self-induced velocity contributions (7) are included in the equations and an adaptive explicit time stepping method is developed to improve both the stability and the accuracy of computations.

The explicit time stepping method is based on *truncated* Taylor series expansions expressed in Lagrangian form for both the position and the vorticity value of individual vortex elements (Grilli and Subramanya [15, 16]). In the present case, second-order Taylor series are used for time updating of both the sheet geometry and the vorticity as,

$$
\begin{aligned}
x_i(t+\Delta t) &= x_i(t)\ \Delta t\,\frac{dx_i}{dt}(t) + \frac{(\Delta t)^2}{2}\,\frac{d^2x_i}{dt^2}(t) + \mathcal{O}[(\Delta t)^3] \\
y_i(t+\Delta t) &= y_i(t)\ \Delta t\,\frac{dy_i}{dt}(t) + \frac{(\Delta t)^2}{2}\,\frac{d^2y_i}{dt^2}(t) + \mathcal{O}[(\Delta t)^3] \\
\Gamma_i(t+\Delta t) &= \Gamma_i(t)\ \Delta t\,\frac{d\Gamma_i}{dt}(t) + \frac{(\Delta t)^2}{2}\,\frac{d^2\Gamma_i}{dt^2}(t) + \mathcal{O}[(\Delta t)^3] \qquad (22)
\end{aligned}
$$

using the Lagrangian definition of velocities (3),

$$
\begin{aligned}
\frac{dx_i}{dt} &= u_i \quad ; \quad \frac{dy_i}{dt} = v_i \\
\frac{d^2x_i}{dt^2} &= \frac{du_i}{dt} \quad ; \quad \frac{d^2y_i}{dt^2} = \frac{dv_i}{dt} \qquad (23)
\end{aligned}
$$

where velocities (u_i, v_i) are given by Eqs. (6) and (7), accelerations $(du_i/dt, dv_i/dt)$ are given by the expressions derived in [14], and rates of change of circulation $d\Gamma_i/dt$ are given by Eqs. (19) and (20), with contributions of semi-infinite vortex sheets of the type (21) being added to the equations for the velocity and the acceleration as detailed above.

As previously noted, equations for $(du_i/dt, dv_i/dt)$ and $d\Gamma_i/dt$ are coupled and therefore must first be solved simultaneously at time t, before accelerations and rates of change of circulation can be used for time stepping of the VS's geometry and vorticity to time $(t + \Delta t)$, using Eqs. (22) and (23). Also note that second derivatives of circulation needed in Eq. (22) are calculated based on backward finite differences as,

$$
\frac{d^2\Gamma_i}{dt^2} \simeq \frac{1}{\Delta t}\left\{\frac{d\Gamma_i}{dt}(t) - \frac{d\Gamma_i}{dt}(t-\Delta t)\right\} \qquad (24)
$$

Following a similar approach as in Grilli and Subramanya [15, 16], the time step Δt used in the model is *adaptively* calculated at each time step based on a constant mesh Courant number

$\mathcal{C}_o$ such that,

$$\Delta t = \mathcal{C}_o \, \frac{\mathrm{Min}(\Delta s_i)}{\mathrm{Max}(\mid \boldsymbol{u}_i \mid)} \tag{25}$$

where the numerator represents the minimum length and the denominator represents the maximum velocity of vortex elements at the current time t. A value $\mathcal{C}_o \simeq 0.5$ ensured good accuracy and stability of computations in most cases.

Computation of geometry and tangential derivatives

In earlier studies (e.g., Zalosh [30]), simple low-order finite difference approximations were used to calculate tangential derivatives along the interfaces [8]. For the problems solved in the present study, however, due to the intense roll-up of vortex sheets that occurs when instabilities develop along the oil-water interface, it is necessary to use a higher-order representation of the geometry along interfaces, even if a lower-order (piecewise-constant) representation is satisfactory for the vorticity. Roll-up indeed leads to a large curvature of the interface and to enhanced surface tension effects (proportional to second-order tangential derivatives of the slope angle; see Eq. (19)) which must be accurately represented. Hence, the interfacial slope and the curvature must be continuous between vortex elements which requires using a piecewise representation of the geometry of third-order or higher.

A higher-order representation of the geometry can be achieved along a segment of an interface either by defining a sliding polynomial interpolation of the geometry on center nodes of the vortex elements or by using a cubic spline fit on these nodes. In the model, sliding polynomials are 5-node 4th-order isoparametric boundary elements in which geometric characteristics are calculated for the middle node of the polynomial. Angles β_i and tangential derivatives $\partial/\partial s$ are calculated along the vortex sheets by direct differentiation of the polynomials. To calculate characteristics for the next node along the interface, the sliding polynomial element is moved forward by one node. The polynomial is identical for the first 3 nodes and for the last 3 nodes on a sheet. With cubic splines, 2-nodes cubic polynomials are defined in such a way as to maintain continuity of the slope from one polynomial to the other. This method, however, requires knowledge of end slopes on the interface to be used as boundary conditions in the spline analysis. Moreover, due to the multiple-valued interface geometry that occurs during roll-up, it is necessary to simultaneously use two parametric spline approximations of the geometry.

Details about both methods can be found in Grilli and Subramanya [16]. In the applications, the sliding and the spline methods are used either individually or in combination. In the latter case, a *hybrid interpolation method* is defined which combines the advantages of both methods to achieve optimal accuracy : (i) the *sliding* method is used first to calculate the slope at both extremities of the computational domain representing an interface; and (ii) the *spline* method is then applied to the whole interface, using the slopes computed in (i) as boundary conditions at both extremities.

More specifically, using either one of the interpolation methods, the angle β along the interface can be expressed as a piecewise analytic expression. Following a classical Boundary Element methodology (e.g., Brebbia [5]), we define the intrinsic coordinate $\mu \in [-1, +1]$ using a piecewise sliding or cubic polynomial interpolation. Under this representation, $x(\mu), y(\mu)$

[8] This is likely another reason why Zalosh could not follow the time development of interfacial instabilities for very long.

and $s(\mu)$ are expressed in closed form within each piecewise polynomial approximation of the geometry of an interface, only as a function of node coordinates. For the geometric parameters in the model, we obtain,

$$\cos\beta = \frac{x_\mu}{s_\mu} \quad , \quad \sin\beta = \frac{y_\mu}{s_\mu} \quad , \quad s_\mu = \{x_\mu^2 + y_\mu^2\}^{1/2} \tag{26}$$

and, for the curvature and its gradient along s,

$$\begin{aligned} \frac{\partial\beta}{\partial s} &= \frac{x_\mu y_{\mu\mu} - x_{\mu\mu} y_\mu}{s_\mu^3} \\ \frac{\partial^2\beta}{\partial s^2} &= \frac{1}{s_\mu^5}\left\{ s_\mu \left(y_{\mu\mu\mu} x_\mu - x_{\mu\mu\mu} y_\mu \right) - \frac{3}{s_\mu}\left[x_{\mu\mu} y_{\mu\mu} \left(x_\mu^2 - y_\mu^2 \right) - x_\mu y_\mu \left(x_{\mu\mu}^2 - y_{\mu\mu}^2 \right) \right] \right\} \end{aligned} \tag{27}$$

respectively, in which indices denote total derivatives with respect to the intrinsic coordinate. Note that, in the second equation (27), third derivatives of the geometry are needed to calculate curvature gradients along the interfaces. This justifies using at least cubic polynomials for the representation of the geometry. In fact, in the applications, to improve the accuracy of computed curvature gradients when cubic splines are used, the third derivatives in (27) are calculated within a (second) spline approximation directly based on the first-derivatives, x_μ and y_μ.

3 Applications

The complexity of the oil containment problem makes it difficult to independently test model results, for both accuracy and convergence, on fully realistic test cases. Moreover, there is not, to our knowledge, any detailed experimental data available for oil slick evolution that could directly be compared with model predictions.

Hence, validation and testing of the principal numerical algorithms in the model is first performed through the solution of the idealized case of a periodic Kelvin-Helmholtz (KH) instability, for which a number of interesting studies can be found in the literature (e.g., Drazin [10], Drazin *et al.* [11], Van de Vooren [25], Rangel and Sirignano [23], Zalosh [31]). Furthermore, as discussed in the introduction, since most failures of contained slicks are initiated by small scale KH instability at the oil-water interface, the periodic KH problem has physical features similar to the oil containment failure problem.

The pure headwave instability of a semi-infinite oil slick in deep water is solved next (i.e., for a slick without a boom), in a set-up similar to the study by Zalosh [30] and Zalosh and Jensen [32] (which used an equivalent but less accurate model). This case illustrates the formation of the headwave which initiates containment failure by critical accumulation.

Application to oil containment by a boom is presented in Section 4, to give an idea of the potential of the Phase I model to solve more complex problems typical of the deployment of real booms.

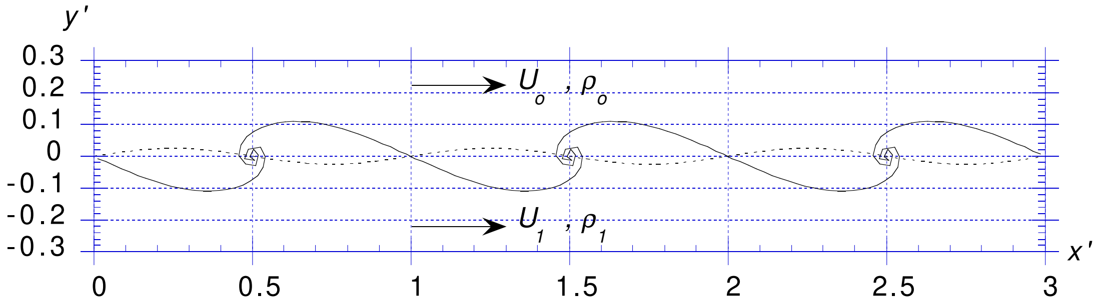

Figure 5: Sketch of computational set-up for periodic Kelvin-Helmholtz instability with wavelength λ (with, $x' = x/\lambda$, $y' = y/\lambda$). U_o, U_1 are uniform velocities and ρ_o, ρ_1 are densities, of fluid 0 and 1, respectively. Curve (- - - -) is the initial sinusoidal perturbation on the interface between fluid 0 and 1 and (———-) is the unstable interface shape computed at a later time (see Fig. 6 (d)).

3.1 Periodic KH instability

The instability patterns observed at the oil-water interface below an oil slick contained by a boom are in many ways similar to a periodic KH instability of small interfacial shear waves (see Section 1). Figure 5 illustrates the periodic KH problem, showing both the initial sinusoidal interfacial waves and (breaking) waves occurring at a later time, due to KH instability and roll-up of the interface VSs.

In order to simulate the KH problem, the equations in the Phase I model had to be modified to account for periodicity of both lateral boundary conditions and integrals and CPV singularities in the Biot-Savart's law. Most of the numerical procedures, however, were unchanged (e.g., for time updating of geometry and vorticity in the interface) and thus could be tested and validated in this application. In the following, we briefly explain how the model was modified to address the periodic KH problem (see details in Grilli *et al.* [14]) and give results of computations for two selected sets of parameter values.

Equations for periodic KH problem

In the periodic KH problem, we consider a two-layer stratified system of infinite extent in the x direction, consisting of two homogeneous inviscid fluids with density ρ_o (e.g., the oil) and ρ_1 (e.g., the water) moving at uniform horizontal velocity U_o and U_1, respectively (Fig. 5). An initial sinusoidal disturbance of wavelength λ, $\eta(x) = \varepsilon \sin(2\pi x/\lambda)$, is specified on the interface between the fluids, with the initial vorticity distribution corresponding to the velocity discontinuity across the interface.

This problem was solved by Lamb [19] in a linearized framework (see p. 373 and p. 461; see also Leibovich [21]). Lamb found that a periodic disturbance would always be unstable and grow exponentially with time if,

$$\Delta U = \mid U_o - U_1 \mid > \frac{1+s}{\sqrt{s}}\, c_o \tag{28}$$

where,

$$c_o = \left(\frac{1}{1+s} \{(1-s)\frac{g}{k} + \sigma_{o1}\frac{k}{\rho_1}\} \right)^{1/2} \tag{29}$$

is the speed of propagation of interfacial waves, $k = 2\pi/\lambda$ is the wavenumber of the interfacial perturbation waves, $s = \rho_o/\rho_1$, and σ_{o1} is the interfacial tension coefficient.

Another way of expressing condition (28) is to define a nondimensional wavenumber W such that,

$$W = \frac{(1+s)^2}{s} \frac{c_o^2}{(\Delta U)^2} \; < \; 1 \tag{30}$$

According to Eq. (28) or (30), the (linear) growth of the instability is maximum for a minimum value of c_o. Calculating $dc_o/dk = 0$ in Eq. (29), we see that a minimum value is achieved for a wavelength,

$$\lambda_m = 2\pi \left(\frac{\sigma_{o1}}{\rho_1 g\,(1-s)} \right)^{1/2} \tag{31}$$

and takes the value,

$$c_{om} = \left(\frac{2}{1+s} \sqrt{\frac{\sigma_{o1}}{\rho_1}\, g\,(1-s)} \right)^{1/2} \tag{32}$$

the critical interfacial wave velocity.

If we select $\lambda = \lambda_m$ as the wavelength of the interfacial instability and $W = W_m = 1$ (given by Eq. (30), with $c_o = c_{om}$), we can calculate the critical velocity discontinuity causing instability ΔU_{cr} and see whether there is (linear) instability or not, for the specified ΔU. We thus obtain,

$$\Delta U_{cr} = \left(2\, \frac{1+s}{s} \sqrt{\frac{\sigma_{o1}}{\rho_1}\, g\,(1-s)} \right)^{1/2} \tag{33}$$

Lamb's solution assumes that the height of the interfacial waves is infinitesimal. This is only an approximation, particularly if the instability is free to develop for a long enough time. This solution, however, can be used to predict the threshold velocity discontinuity ΔU_{cr} likely to cause initial instability of interfacial waves. Moreover, despite their limitations, Lamb's equations contain all the correct physical parameters known to influence interfacial instability in the oil containment problem (i.e., fluid density ratio, interfacial tension, and gravity).

Rangel and Sirignano [23] computed the nonlinear periodic KH instability problem, including surface tension effects (but not gravity), and found that Lamb's linear solution only gave the correct growth rate of the interfacial waves for short times. For sufficiently long time, the amplitude of interfacial waves increased and nonlinearity provided additional stabilizing effects that slowed the growth of the instability. Furthermore, they showed that maximum growth was achieved in the nonlinear case when $W = 2/3$.

For a periodic problem with wavelength λ, it can be shown that Biot-Savart's law transforms into (e.g., Van de Vooren [25], Grilli *et al.* [14]),

$$\begin{aligned} u_i &= \frac{1}{2\lambda} \sum_{j \neq i} \Gamma_j \frac{\sinh 2\pi(y'_i - y'_j)}{\cosh 2\pi(y'_i - y'_j) - \cos 2\pi(x'_i - x'_j)} \; + \; \tilde{u}_i \\ v_i &= -\frac{1}{2\lambda} \sum_{j \neq i} \Gamma_j \frac{\sin 2\pi(x'_i - x'_j)}{\cosh 2\pi(y'_i - y'_j) - \cos 2\pi(x'_i - x'_j)} \; + \; \tilde{v}_i \end{aligned} \tag{34}$$

for $(i, j = 1, ..., N)$, where dimensionless variables, $x' = x/\lambda$ and $y' = y/\lambda$, have been used.

In Eq. (34), as in Eq. (6), the interface has been assumed to be discretized by N segments with piecewise-constant vorticity density γ_j. Velocities $\tilde{u}_i$ and $\tilde{v}_i$ denote CPV integrals resulting from singularities occurring when the source point (x_i, y_i) coincides with the integration point (x_j, y_j) (i.e., self-induced velocity contributions). To our knowledge, since most existing models assume a discretization using (less accurate) point vortices, these periodic CPV integrals have never been exactly calculated in the literature. Only Van de Vooren [25] provided a first-order approximation for these, based on a Taylor series expansion of the singularities. Full expressions for $\tilde{u}_i$ and $\tilde{v}_i$ can be found in Grilli *et al.* [14].

Using linear theory, the initial distribution of vorticity can be calculated for the initial sinusoidal interface as $(i = 1, ..., N)$,

$$\gamma_i = \frac{1}{N\Delta s_i}\left(1 + 2\pi\varepsilon\left\{\kappa\sin(2\pi x_i') - 2\frac{\sqrt{s(1-W)}}{(1+s)}\cos(2\pi x_i')\right\}\right) \tag{35}$$

where κ is the Atwood number defined earlier, ε is the initial amplitude of the interfacial wave, and W (< 1) is given by Eq. (30) for the selected values of the physical parameters.

Equation (35) was used by Rangel and Sirignano [23], with $g = 0$, to specify initial vorticity in their solution of KH instability problems [9].

If the two-fluid system is made of identical fluids with different velocities, we have $s = 1$, $\kappa = 0$, and $W = 0$ and, hence, the initial vorticity density is given by,

$$\gamma_i = \frac{1}{N\Delta s_i}\{1 - 2\pi\,\varepsilon\,\cos(2\pi x_i')\} \tag{36}$$

Zalosh [31] used this simpler equation to specify the initial vorticity distribution in his solution of the KH-problem. Since he used two different fluids, however, this led to an incorrect specification of the initial disturbance, which might partly explain why he could not achieve sufficient accuracy and stability in his computations.

Summary of computational techniques

A computational test case for the KH instability problem is defined by selecting values of physical parameters : $\rho_o, \rho_1, \Delta U$, and σ_{o1}. Due to the spatial periodicity of the KH problem (e.g., Fig. 5), a domain representing only one wave length λ is modeled in the computations (e.g., Figs. 6 and 7) and numerical parameters are selected as : (i) the initial number N of piecewise-constant vortex elements on the interface, of initial length $\Delta s_o \simeq \lambda/N$; and (ii) the initial time step, Δt_o. The latter is found according to Eq. (25), in which we assume that the initial sheet velocity is, by definition (see [3]), the average of fluid 0 and 1 velocities, i.e., $\Delta U/2$ (for $U_o = 0$ in the present case), and the Courant number $\mathcal{C}_o = 0.5$; we thus obtain, $\Delta t_o = \lambda/(N\Delta U)$.

The initial vorticity distribution on the interface is calculated using Eq. (35) for a two-fluid system (second application below) and Eq. (36) for a problem with the same fluid for both layers (first application below). In the present computations, as in Rangel and Sirignano [23],

[9] Note that, in this study, computations were carried out using an incorrect coefficient in the equation for time updating of the vorticity (i.e., similar to Eq. (19)); this was later corrected by Rangel and Sirignano [24].

we use $\varepsilon = 0.025$ to define the initial perturbation on the interface and the initial shape of the interface is selected as $\eta(x) = \varepsilon \sin(2\pi x/\lambda)$.

Due to periodicity, corner points at both extremities of the modeled interface-sheet (i.e., points 1 and N) must always behave similarly in the computations, i.e., have the same y-coordinates, x-coordinates separated by λ, and identical velocity, acceleration, and vorticity. Lateral boundary conditions are used to "enforce" these requirements. For instance, horizontal coordinates are constrained as,

$$(x_N - x_1) + \Delta s_{1/2} \cos\beta_1 + \Delta s_{N+1/2} \cos\beta_N = \lambda \tag{37}$$

The interface evolution is tracked as a function of time by iteratively using the explicit time updating procedure (22)-(24). For each time step, the velocity on the interface is calculated using Eqs. (34), with the expressions of the CPV induced velocities from [14], and the acceleration is calculated using time derivatives of these equations.

Tangential derivatives along the interface are calculated using both the 4th-order sliding elements and the spline procedures. In the present computations, the hybrid interpolation method is used in combination with periodicity conditions expressed between nodes $(1 + j)$ and $(N - j)$, $(j = 0, ..., 3)$ of the computational domain. This hybrid interpolation method was found to eliminate errors and instabilities of the solution that were first observed, particularly at both extremities of the interface, when only one of the above methods was used.

Computational results

Computations were performed for two cases, using $U_o = 0$ (i.e., a still upper layer) and $U_1 = 0.25$ m/s (which is larger than the critical value for oil/water of about 0.15 m/s; see below) : (i) $s = \rho_o/\rho_1 = 1$ (water/water interface; same fluid) and no surface tension ($\sigma'_{o1} = 0$); and (ii) $s = 0.90$ (light oil/water interface; two-fluid system) and an average surface tension $\sigma'_{o1} = 0.0237$ N/m (oil/water value). $N = 55$ piecewise-constant vortex elements were first used to discretize the interface for both cases. Figure 6 (a) shows the locations of nodes between the vortex elements in the discretization after 11 time steps.

In the first case (i), with a water-water system, Eq. (19) would show that $d\Gamma_i/dt = 0$, i.e., the vorticity, is constant as a function of time (which in fact follows from Kelvin's theorem; Eq. (11)). This case in fact represents a very unstable limiting case for KH instability computations (Rangel and Sirignano [23]); one for which the instability grows with the same time rate for any wavelength. For this case, due to the absence of surface tension and density difference at the interface, the analysis of the most unstable wavelength λ_m presented above is irrelevant. Hence, λ can be arbitrarily selected and results for any wavelength are expected to be self-similar. To confirm this, computations were performed for $\lambda = 0.01$, 0.1, 1, and 5 m. Non-dimensional interface profiles were found to be close to identical in all cases, as a function of non-dimensional time $\tau = t\Delta U/\lambda$. In the following, we present results obtained for case (i) with $\lambda = 1$ m (Fig. 6). For this value, the initial time step is $\Delta t_o = 0.0727$ s (or $\Delta\tau_o = 0.01818$; in fact the nondimensional time step is independent of wavelength).

In the second case (ii), following the linear analysis, the wavelength is set from Eq. (31) to $\lambda = \lambda_m = 0.0309$ m, which provides the maximum growth rate of the (linear) instability. This gives a value $\lambda = 0.0309$ m and, hence, $\Delta t_o = 0.00225$ s or $\Delta\tau_o = 0.0182$ (note that dimensionless time steps are identical to $1/N$ for both cases (i) and (ii)). This small

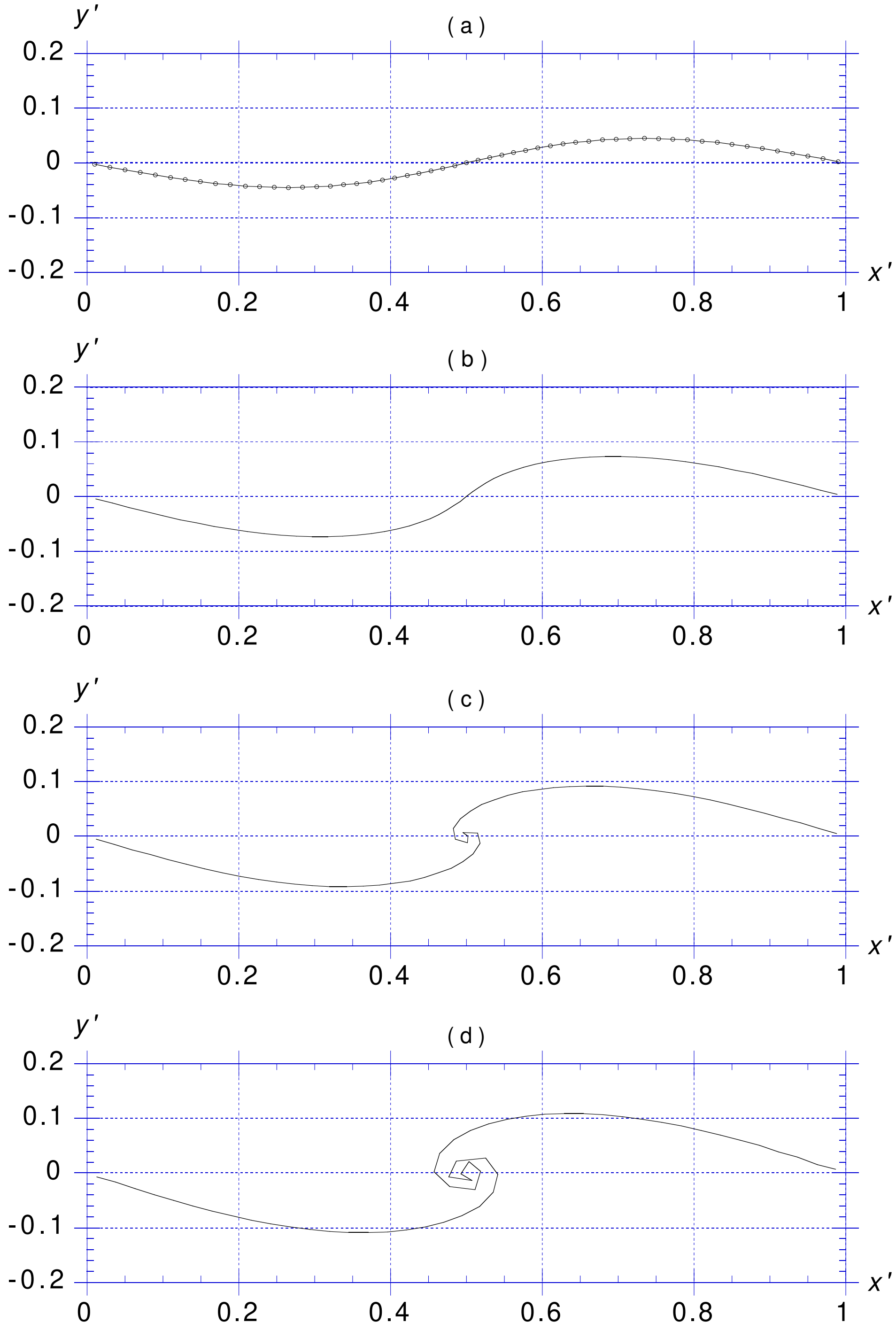

Figure 6: Interface shape $x' = x/\lambda$ and $y' = y/\lambda$ for KH instability computations in a set-up similar to Fig. 5 with $U_o = 0$ and $U_1 = 0.25$ m/s, $\rho_o/\rho_1 = 1$ (same fluid) and $\lambda = 1$ m and no surface tension. The initial time step is $\Delta t_o = 0.0727$ s and the initial perturbation is a sinusoidal wave with vorticity distribution according to Eq. (36), with $\varepsilon = 0.025$. Results are for $t =$ (a) 0.8; (b) 1.53; (c) 1.91; and (d) 2.24 s; corresponding to 11, 21, 31, and 43 varying time steps, respectively. The interface was discretized using $N = 55$ piecewise-constant vorticies and $\mathcal{C}_o = 0.5$. ($\circ$) in figure (a) denote nodes between vortex elements.

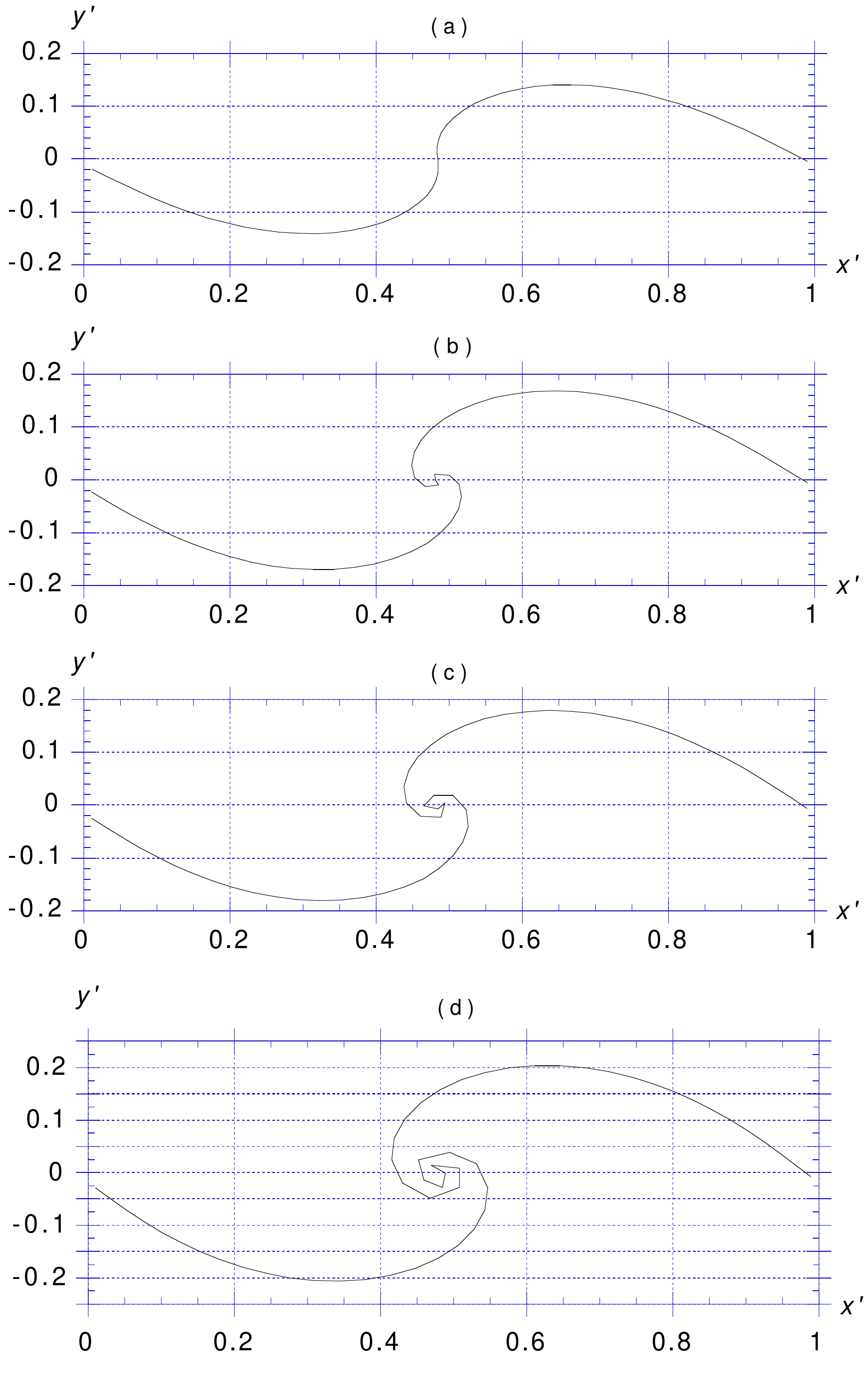

Figure 7: Same results as in Fig. 6 for $\rho_o/\rho_1 = 0.9$, a surface tension $\sigma_{o1} = 0.0237$ N/m, and $\lambda = 0.031$ m (water-oil; ripple scale). The initial time step is $\Delta t_o = 0.00225$ s and the initial perturbation is as in Fig. 6, with the initial vorticity distribution from Eq. (35). Results are for $t =$ (a) 1.74; (b) 1.85; (c) 1.89; and (d) 1.98 10^{-2} s; again corresponding to 6, 12, 16, and 22 varying time steps, respectively.

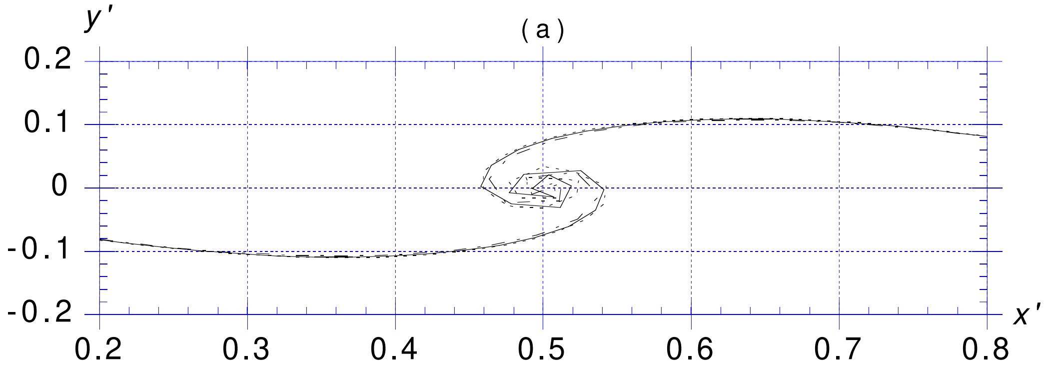

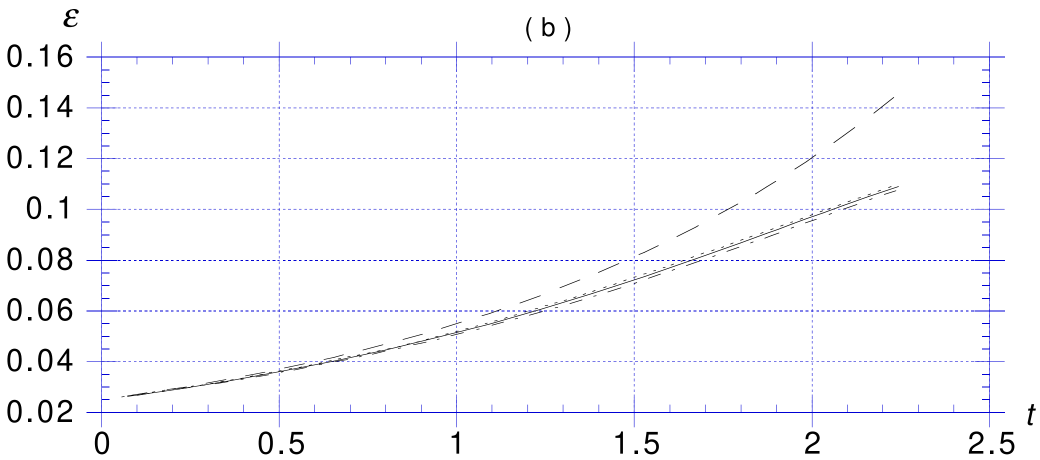

Figure 8: Same computations as in Fig. 6 for N = (— - —) 40; (——) 55; and (- - - - -) 70, vortex elements on the interface; with : (a) interface shape at $t = 2.24$ s; (b) growth of interfacial amplitude ε as a function of time t compared to (— —), the linear growth rate (Lamb [19]).

wavelength corresponds to an instability at the ripple scale (with $c_{om} = 0.0712$ m/s from Eq. (32)). As a verification of the (linear) instability of the problem for case (ii), we should obtain $W = W_m = 0.325$ from Eq. (30) and $\Delta U_{cr} = 0.143$ m/s from Eq. (33), i.e., the result gives $W < 1$ and $\Delta U > \Delta U_{cr}$.

Results in Figs. 6 and 7 show interface profiles typical of the KH instability, with overturning and intense roll-up of the vortex sheet on the interface. In the first case, the time step remains approximately equal to its initial value for 23 time steps, up to $t = 1.67$ s (i.e., just slightly beyond the time of Fig. 6 (b)). For later time, due to the overturning of the interfacial wave and the resulting shortening of the vortex elements length, however, the time step value progressively reduces according to the adaptive time step Eq. (25), and reduces to $\Delta\tau = 0.00926$ at $t = 2.24$ s (Fig. 6 (d)). A similar variation in time step size is observed for the second case. Note that, in earlier works by Zalosh [31] and Rangel and Sirignano [23], a constant time step value was used. This prevented adjusting the level of accuracy in their models when interfacial instabilities occurred.

Overall, for both cases, numerical results are smooth and well-behaved, even when vortex sheet elements are very close to each other (see, e.g., Figs. 6 and 7 (d)). This confirms the correct treatment of the CPV singularities in the model.

For both cases in Figs. 6 and 7, the number of vortex elements on the interface was first decreased to $N = 40$ (from $N = 55$) and then increased to $N = 70$. The initial time step was adjusted accordingly. Computations were performed for these lower and higher level discretizations. Figure 8 (a) shows a comparison of free surface shapes obtained at $t = 2.24$ s for the same case as in Fig. 6 and the three selected discretizations. The agreement between the three is quite good, except in the small central region where intense roll-up of the VSs occurs. Figure 8 (b) shows the evolution of the interfacial amplitude as a function of time, for the three discretizations. For both the finer and the coarser discretizations, interfacial amplitudes stay within 2% of the results for $N = 55$. Hence, results are not significantly affected by a slight decrease or increase in resolution. This confirms both the convergence and the stability of the numerical model, particularly compared to earlier works [31, 23] where computed results showed irregular behavior when the size of the vortex elements was too small. Also, note the differences in Fig. 8 (b) between the amplitude growth rates obtained with the present nonlinear model and the rate predicted by linear theory (Lamb [19]; in fact here simply, $\propto \exp(\pi \Delta U t/\lambda)$). Clearly, for sufficiently long times, nonlinearity increases and the instability grows slower in the nonlinear model than predicted by linear theory. This confirms earlier findings [31, 23] that nonlinearity stabilizes the KH instability.

Finally, comparing both Figs. 6 and 7, one can see that the second case, with oil/water and surface tension, leads to a relatively larger scale of instability (in non-dimensional values, i.e., with respect to the selected wavelength) that also develops at a faster (non-dimensional) rate than in the first case. The interface shape is up/down symmetrical in the first case (Fig. 6), where buoyancy does not play a role ($s = 1$), and slightly asymmetrical in the second case (see Fig. 7 (d)) due to buoyancy effect ($s = 0.9$). The present results are qualitatively similar to those obtained by Rangel and Sirignano [23]. The latter study, however, did not include gravity and used several incorrect coefficients in the vorticity updating equation. Hence, a direct comparison is not feasible.

3.2 Deep water headwave instability

This case corresponds to the problem solved by Zalosh [30] and sketched in Fig. 9. A semi-infinite oil slick with zero initial velocity $U_o = 0$ is subjected to a water flow velocity U_w (and an air flow U_a). An instability soon develops in front of the slick, and propagates downstream as a headwave. The wave quickly overturns and rolls-up on itself in a way similar to KH instability waves calculated in the previous section (Figs. 6 and 7).

Computational model and initial slick shape

In the following, we explain how the model was used to solve the headwave instability problem (particularly the selection of the initial slick shape) and give results for two cases similar to those modeled by Zalosh [30].

The computational model used for this case is the original model introduced in Section 2. In the solution, three semi-infinite VSs (si) were used to represent both the up and downstream

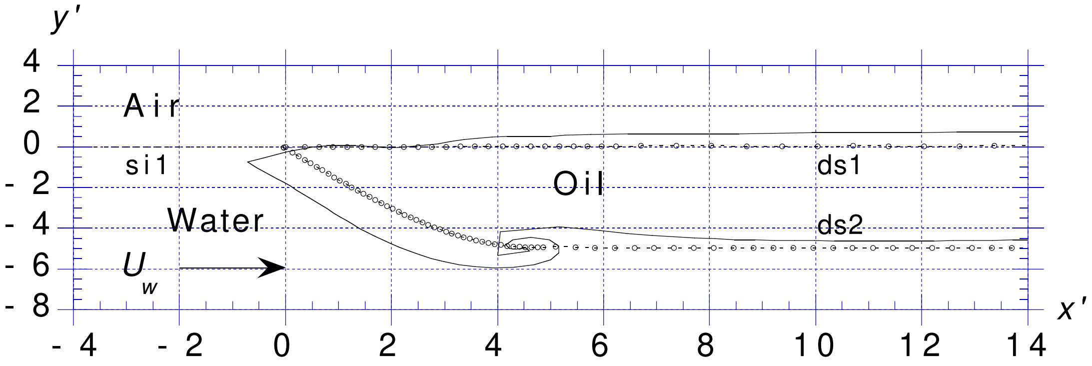

Figure 9: Sketch of computational domain for headwave instability of a semi-infinite oil slick, with definition of main parameters : U_w = water velocity with respect to slick ($U_o = 0$); air velocity can be set to U_a and interfacial tensions to σ_{oa} and σ_{ow}; densities are $\rho_a = 0$, ρ_o and ρ_w; si1, and si2, si3 (not shown) = three semi-infinite vortex sheets; ds1, ds2 = piecewise-constant discretized vortex sheets; $\circ$ = centers of discretized vortex elements. (- - - - -) initial shape of the slick; (———-) unstable headwave at a later time (see Fig. 10 (d)).

portions of the oil and water domains, and two VSs discretized with piecewise-constant vortex elements (sd) were used to represent the oil-water and oil-air interfaces (Fig. 9).

Note that, to overcome problems caused by the lack of representation of the self-induced velocities and other shortcomings in his model, Zalosh introduced the concept of a viscosity-core in which contributions of individual point vortices in the discretized Biot-Savart equations (2) were multiplied by a term of the form $[1 - \exp(-r_{ij}^2/R_c^2)]$ (in which R_c is the "core radius") providing a very small contribution to the velocity field for point vortices j's very close to point i. Zalosh stated that his numerical model was unstable without the use of this "damping" method. After experimenting with this method, we found that it was not needed for our model to provide both stable and accurate results, except at the three intersections between semi-infinite sheets and the piecewise-constant vortex sheets. This was thought to be due to the local mismatch between the continuous vorticity on the semi-infinite sheets and the piecewise-constant vorticity on the discretized vortex sheets. This problem will likely be eliminated in the improved version of the Phase I model which is being developed as a continuation of this study—the Phase II model—, in which higher-order vortex elements will be used for the discretization of vortex sheets. For the three intersection points, a core length equal to the distance to the first vortex element center is used.

The *initial slick shape* was selected as in Zalosh (see Fig. 9), based on the observation of various experimental results,

$$\begin{aligned} \eta(x) &= D \sin(2\pi\, x/L) \qquad && \text{for } 0 \le x \le L/4 \\ \eta(x) &= D && \text{for } L/4 \le x \le L \end{aligned} \tag{38}$$

where D and L are the initial depth and length of the slick headwave, respectively. Using Bernoulli's equation between the front and the back of the slick, we obtain,

$$D = \frac{U_w^2}{2g\,(1-s)} \tag{39}$$

Following the work by Von Karman [26] for density intrusions along solid boundaries, Zalosh assumed a 60° value for the angle of the headwave at the leading edge. With this angle, Eq. (38) yields $L = 3.63D$. As pointed out by Zalosh, experimental results usually show smaller angles at the leading edge, and result in increased values of L. In the present case, however, we simply used the same initial shape as Zalosh's to compare our results to those he obtained. Specification of the initial slick shape will be improved in the Phase II model.

Computational results

In the computations, the VSs on the interfaces are discretized using $N_a = 45$ segments with piecewise-constant vorticity between air and oil, and $N_w = 85$ segments between oil and water. To provide a finer discretization in the headwave region where the main instability occurs, for each sheet in the initial discretization, half the vortices are specified with equal x-spacing in the headwave region, i.e., for $0 \leq x \leq L/4$, and the other half are specified with equal spacing in the rest of the slick, i.e., for $L/4 \leq x \leq L$ (see Fig. 9). With this discretization, we have a minimum initial length of vortex elements equal to about $\Delta s_o \simeq L/(2N_w)$ and an initial time step, according to Eq. (25), equal to $\Delta t_o = \mathcal{C}_o L/(N_w U_w)$ (assuming an initial maximum velocity of the oil-water VS equal to $U_w/2$).

Two cases are studied for $s = 0.9$ and 0.75, with an oil-water surface tension $\sigma_{ow} = 0.0237$ N/m. In both cases, the water velocity is set to $U_w = 0.25$ m/s, which is above the critical value for oil and water, and the air velocity is set to $U_a = 0$. A length-scale $\lambda = U_w^2/g = 0.00637$ m is used in the model (defined as in [22, 30]) and the corresponding time scale is $U_w/g = 0.02548$ s. Following Eq. (39), the initial slicks are specified with depth $D' = D/\lambda = 5$ and 2, and length $L' = L/\lambda = 18.15$ and 7.26, for each test case, respectively. With $\mathcal{C}_o = 0.5$, initial time steps are, $\Delta\tau_o = \mathcal{C}_o L'/N_w = 0.107$ and 0.0427, for each case, or $\Delta t_o = 0.00273$ and 0.00109 s, respectively.

Results obtained in Figs. 10 and 11 are qualitatively similar to Zalosh's results but are better resolved in space and the developments of instabilities (roll-up) can be computed for a longer time. Model calculations are found to be both stable and accurate, without need for smoothing the interface or surface geometry, or for other transformations of model outputs used in earlier studies [30, 31, 23].

Results of other computations (not reported here) are also found to be improved in both resolution and duration of computations when a larger number of vorticies are used on the interface. This confirms the accuracy of the CPV integrals computed for the self-induced velocities and demonstrates both the stability and accuracy of the time updating procedures used in the present model.

4 Conclusions and future developments

In this paper, we presented the development and testing of an hydrodynamic model for oil containment by a boom, referred to as the *Phase I model*. To do so, the relevant literature and key physical phenomena relative to oil containment were analyzed. Important parameters were isolated and used to develop a numerical model of interfacial instabilities for a two-phase system consisting of a layer of oil on top of a uniform flowing water stream.

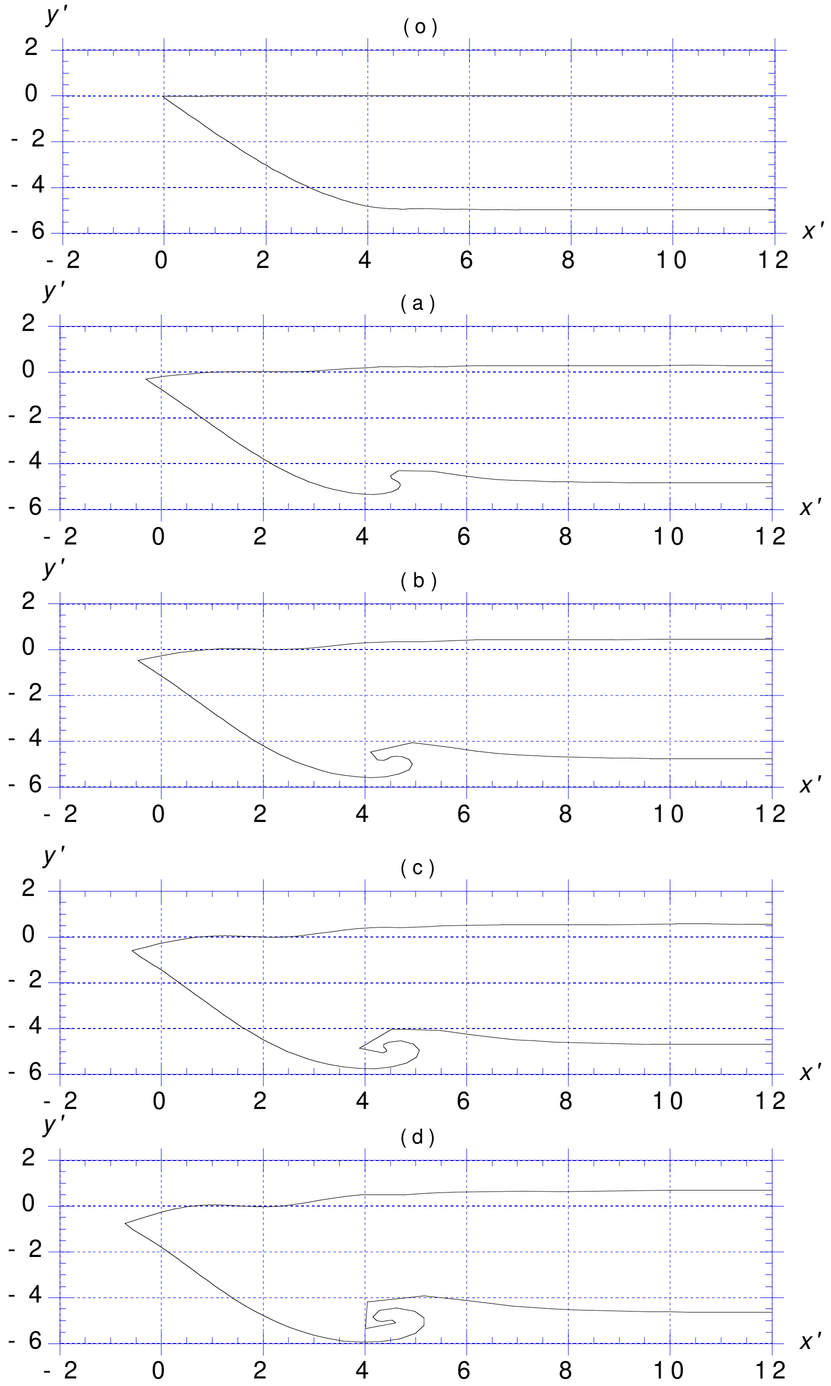

Figure 10: Typical results for headwave instability computations as in Zalosh [30], in the same set-up as in Fig. 9, with $U_w = 0.25$ m/s, $U_o = 0$, $U_a = 0$ m/s, $s = \rho_o/\rho_w = 0.9$, $\sigma_{ow} = 0.0237$ N/m (water-oil). Results $(D' = 5, L' = 18.15)$: (o) shape of the slick after one time step $t = 0.00273$ s; development of instability for $t =$ (a) 1.8; (b) 3.1; (c) 4.1; and (d) 5.2 10^{-2} s; corresponding to 5, 10, 16, and 22 varying time steps, respectively. Three semi-infinite sheets were used and interfaces were discretized with $N_a = 45$ piecewise-constant vorticies between air and oil and $N_w = 85$ between oil and water.

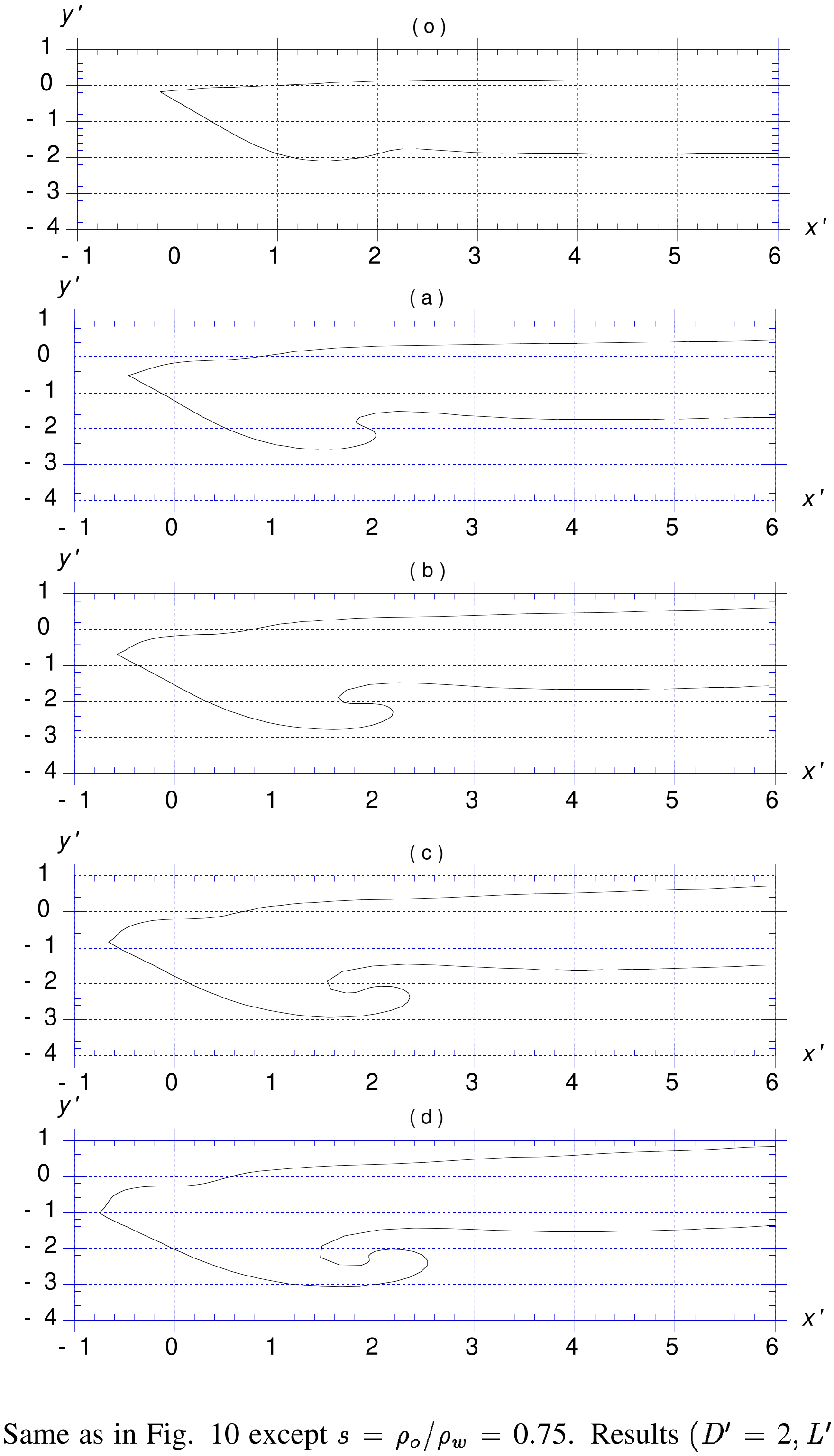

Figure 11: Same as in Fig. 10 except $s = \rho_o/\rho_w = 0.75$. Results $(D' = 2, L' = 7.26)$: (o) shape of the slick after one time step $t = 0.00109$ s; development of instability for $t =$ (a) 0.59; (b) 0.80; (c) 1.06; and (d) 1.30 10^{-2} s; corresponding to 5, 10, 16, and 22 varying time steps, respectively.

This model relied on well-established *Vortex Sheet* dynamics methods with, however, several significant improvements compared to existing work in the literature. Key improvements included,

- the use of piecewise-constant vortex sheets (instead of point vortices) and the inclusion of self-induced velocity terms along the interfaces (with exact calculation of the CPV integrals);
- the use of time updating equations for the sheet vorticity that account for inertial, gravity and surface tension effects;
- the use of a piecewise cubic-continuous representation of the geometry allowing for a more accurate calculation of higher-order tangential derivatives along interfaces;
- the use of a more accurate and stable explicit scheme, with exact calculation of vortex sheet accelerations, for time-updating of both the vorticity and the geometry of the interfaces;
- the use of a self-adaptive, time-stepping method, based on a mesh Courant number.

Applications of the Phase I model presented in Section 3 concentrated principally on studying two somewhat "academic" problems aimed at both testing the accuracy of the numerical procedures implemented in the model and better understanding the physics of unstable two-fluid systems; namely, the periodic Kelvin-Helmholtz instability and the semi-infinite headwave instability of a two-fluid system. These two applications illustrated the capabilities and efficiency of the model. They also gave us a solid basis for performing more complex studies including a boom and other solid boundaries like the bottom.

To carry out the first application (KH problem), model equations had to be re-derived to include the spatial periodicity of the problem. Self-induced velocity terms also had to be expressed for the periodic problem. To our knowledge, such derivations have not been presented in the literature. In the second application to the headwave problem, both for sake of comparison and for simplicity, the initial shape of the oil slick was selected, somewhat arbitrarily, as in the study by Zalosh [30].

Hence, the Phase I model provides a firm foundation with which to perform more sophisticated analyses that are more closely representative of at sea and full-scale laboratory conditions. Such analyses will imply extending the Phase I model to include a more accurate physical representation of interfacial instability. This is the object of a continuation of this project presently in progress, referred to as the *Phase II model*. In particular, *interfacial friction* was identified as one of the important factors for critical accumulation. In the Phase I model, however, no explicit friction term was included in the dynamics of the inviscid VSs. Hence, modeling viscous and turbulent effects within a small boundary layer close to the oil-water interface and thus including friction forces in the analysis will be an essential part of the Phase II model. In the Phase II model, we plan to use higher-order elements to represent VSs and thus provide better accuracy for the representation of interfacial waves. Finally, a new method for accurately calculating the initial steady-state shape of a contained oil slick, based on the hydrodynamic equilibrium equations, will also represent an essential component of the Phase II model.

Future developments for the Phase II model can thus be summarized as follows,

- the study of oil-water-boom systems;

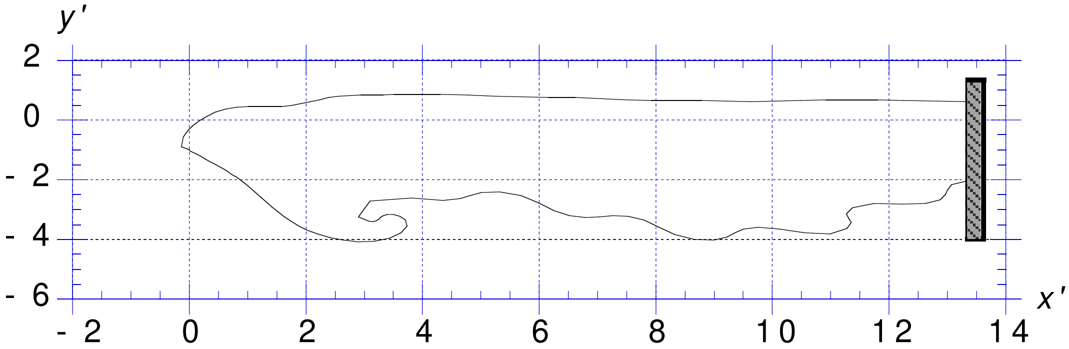

Figure 12: Illustration of computations with Phase I model for an oil slick contained by a boom. In this case, both a headwave and interfacial instabilities simultaneously develop.

- the initialization of the steady-state oil slick based on a solution of the hydrodynamic equilibrium equations;
- computation of friction along the oil-water interface, both for the initialization of the slick shape and for the time updating of the slick geometry and dynamics; these computations will include both viscous and turbulent diffusion effects within boundary layers close to the interfaces;
- using viscous/turbulent vortex sheets combining a local Navier-Stokes solver with turbulent closure models ($k - \varepsilon$ or similar);
- using higher-order vortex elements to provide better accuracy of computations along interfaces (i.e., use of non-constant vortex elements in the BEM);
- performing a broad parametric study of critical accumulation failure modes with validation of computational results by comparison to experimental results; and
- a tentative optimization of boom/barrier systems by varying geometrical and physical parameters of the problem.

To give an idea of future problems addressed in this study, Fig. 12 illustrates computations involving a solid boom and an oil slick. These computations had used physical parameter values similar to those for the case shown in Fig. 10, with the addition of an harmonic "noise", superimposed on the interfacial motion, to represent ocean wave action. Although these computations were performed with the Phase I model, i.e., without both the accurate slick initialization and the numerical improvements planned for the Phase II model, one can see that we obtain quite a realistic picture of interfacial instabilities such as those observed in laboratory experiments, namely, the occurrence of both a headwave and interfacial waves propagating along the oil-water interface and reflecting off the boom.

Acknowledgments

This work was supported by the U.S. Department of Transportation, Grants No. DTRS57-94-G-00076 and DTRS57-95-G-00065, under the Oil Pollution Research Grant Program. The able assistance of John Putukian, Volpe National Transportation Systems Center, Boston, Massachusetts, contracting officer's representative, and the enthusiastic support of Ken Bitting, U.S. Coast Guard Research and Development Center, Groton, Connecticut, are gratefully acknowledged. Andrie Chen, Exxon Production Research, Houston, Texas, served as an industrial technical advisor to the project.

References

[1] Agrawal, R.K. and Hale, L.A. 'A new criteria for predicting head wave instability of an oil slick by a barrier', *Proc. Offshore Tech. Conf.,* Dallas, Texas, pps. 461-466, 1974.

[2] Bai, K.J. and Kim, J.W. 'A computational model for flow around an oil boom', *Proc. Workshop on Tidal and Oil Spill Modeling,* 5-17, 1993.

[3] Batchelor, G. K., *An introduction to fluid dynamics* Cambridge University Press, 1967.

[4] Benjamin, T.B. 'Gravity currents and related phenomena', *J. Fluid Mech.,* **31** (2), 209-248, 1968.

[5] Brebbia, C.A., *The Boundary Elements for Engineers* John Wiley and Sons, 1978.

[6] Clavelle, E.J. and Rowe, R.D. 'Numerical simulation of oil–boom failure by critical accumulation', *Arctic Marine Oil Spill Prog. Tech. Seminar,* 409-418, 1993.

[7] Cross, R.H. and Hoult, D.P. 'Oil booms in tidal currents', *J. Waterways, Port. Coastal Ocean Engng.,* **98**, 1745-1758, 1972.

[8] Delvigne, G.A.L. 'Barrier failure by critical accumulation of viscous oil', *Proc. Oil Spill Conf.,* USEPA, USCG, and Amer. Petrol. Inst., pps. 143-148, 1989.

[9] Di Pietro, N. D. and Cox, R. G. 'The containment of an oil slick by a boom placed across a uniform stream', *J. Fluid Mech.,* **96,** 613-640, 1980.

[10] Drazin, P.G. 'Kelvin-Helmholtz instability of finite amplitude', *J. Fluid Mech.,* **42,** 321-335, 1970.

[11] Drazin, P.G. and Howard, L.N. 'Hydrodynamic stability of parallel flow of inviscid fluid', *Advanc. Applied Mech.,* **9,** 1, 1966.

[12] Ertekin, R.C. and Sundararaghavan, H. 'The calculation of the instability criterion for a uniform viscous flow past a boom', *J. Offshore Mech. Artic Engng.,* **117,** 24-29, 1995.

[13] Fink, P.T. and Soh, W.K. 'Calculation of vortex sheets in unsteady flow and application in ship hydrodynamics', *Proc. 10th Symp. on Naval Hydrodynamics,* Office of Naval Res., Washington, D.C., 463-491, 1974.

[14] Grilli, S.T., Hu, Z., and Spaulding, M.L. 'A hydrodynamic model of oil containment by a boom : Phase I', *Final Technical Report for DOT Grant No. DTRS57-94-G-00076*, Dept. Ocean Engng., Univ. of Rhode Island, 70pps, 1996.

[15] Grilli, S.T. and Subramanya, R. 'Recent Advances in the BEM Modelling of Nonlinear Water Waves'. Chapter 4 in *Boundary Element Applications in Fluid Mechanics* (ed. H. Power), pps. 91-122. Advances in Fluid Mechanics Series. Computational Mechanics Publication, Southampton, UK, 1995.

[16] Grilli, S.T. and Subramanya, R. 'Numerical modeling of wave breaking induced by fixed or moving boundaries.' *Computational Mechanics* **17** (in press), 1996.

[17] Johnston, A.J., Fitzmaurice, M.R. and Watt, R.G. 'Oil spill containment : viscous oils', *Proc. Oil Spill Conf. (USEPA, USCG),* Amer. Petrol. Inst., pps. 89-94, 1993.

[18] Jones, W. T. 'Instability at an interface between oil and flowing water', *J. of Basic Engng.,* **94,** 874-878, 1972.

[19] Lamb, H. *Hydrodynamics* Cambridge University Press, 6th edition, 1932.

[20] Lau, Y.L. and Kirchifer, S.A. 'A review of the dynamics of contained oil slicks in flowing water', *J. Hydraulics Div.,* 1974.

[21] Leibovich, S. 'Oil slick instability and the entrainment failure of oil containment booms', *J. Fluids Engng.,* **98,** 98-105, 1976.

[22] Milgram, J.H. and Van Houten, R.J. 'Mechanics of a restrained layer of floating oil above a water current', *J. Hydronautics,* **12** (3), 93-108, 1978.

[23] Rangel, R.H. and Sirignano, W.A. 'Nonlinear growth of Kelvin-Helmholtz instability : Effect of surface tension and density ratio', *Phys. of Fluids,* **31** (7),1845-1855, 1988.

[24] Rangel, R.H. and Sirignano, W.A. 'The linear and nonlinear shear instability of a fluid sheet', *Phys. of Fluids.* **A3** (10), 2392-2400, 1991.

[25] Van de Vooren, A.I. 'Numerical investigation of the rolling-up of vortex sheets', *Proc. R. Soc. Lond.,* **A 373**, 67-91, 1980.

[26] Von Karman T., 'The engineer grapples in the nonlinear problems', *Bull. Am. Math. Soc.* **46**, 615-586, 1940.

[27] Wicks, M. 'Fluid dynamics of floating oil containment by mechanical barriers in the presence of water currents', *Proc. API-FWPCA Joint Conf. on Prevention and Control of Oil Spills,* New York, Dec 15-17, Amer. Petrol. Inst., pps. 55-106, 1969.

[28] Wilkinson, D. L. 'Dynamics of contained oil slicks', *J. Hydraulics Div.,* **98,** 1013-1031, 1972.

[29] Wilkinson, D. L. 'Limitations to length of contained oil slicks', *J. Hydraulic Div.,* **99,** 701-713, 1973.

[30] Zalosh, R.G. 'A numerical model of droplet entrainment from a contained oil slick', *Report No.* **CG-D-65-75**, DOT/USCG, 1974.

[31] Zalosh, R.G. 'Discretized simulation of vortex sheet evolution with buoyancy and surface tension effects', *J. AIAA,* **14**, 1517-1523, 1976.

[32] Zalosh, R.G. and Jensen, D.S. 'A numerical model of droplet entrainment from a contained oil slick', *Proc. Fluid Mech. in Petrol. Indus.,* ASME, 17-27, 1975.

[33] Zaroodny, S.J. and Greenberg, M.D. 'On a vortex sheet approach to the numerical calculation of water waves', *J. Comp. Phys.,* **11**, 440-446, 1973.